Modeling the mechanics of amorphous solids at different length scale and time scale

2011 Modelling Simul. Mater. Sci. Eng. 19 083001

(http://iopscience.iop.org/0965-0393/19/8/083001)

Modelling Simul. Mater. Sci. Eng. **19** (2011) 083001 (49pp) doi:10.1088/0965-0393/19/8/083001

TOPICAL REVIEW

Modeling the mechanics of amorphous solids at different length scale and time scale

D Rodney[1], **A Tanguy**[2] **and D Vandembroucq**[3]

[1] Laboratoire Science et Ingénierie des Matériaux et Procédés, Grenoble INP, UJF, CNRS, Domaine Universitaire BP 46, F38402 Saint Martin d'Hères, France
[2] Laboratoire de Physique de la Matière Condensée et Nanostructures, Université Lyon 1, Domaine Scientifique de la Doua, F69622 Villeurbanne, France
[3] Laboratoire Physique et Mécanique des Milieux Hétérogènes, CNRS/ESPCI/UPMC/Université Paris 7 Diderot, 10 rue Vauquelin, F75231 Paris, France

E-mail: david.rodney@grenoble-inp.fr

Received 5 June 2011, in final form 9 September 2011
Published 3 November 2011
Online at stacks.iop.org/MSMSE/19/083001

Abstract
We review the recent literature on the simulation of the structure and deformation of amorphous solids, including oxide and metallic glasses. We consider simulations at different length scale and time scale. At the nanometer scale, we review studies based on atomistic simulations, with a particular emphasis on the role of the potential energy landscape and of the temperature. At the micrometer scale, we present the different mesoscopic models of amorphous plasticity and show the relation between shear banding and the type of disorder and correlations (e.g. elastic) included in the models. At the macroscopic range, we review the different constitutive laws used in finite-element simulations. We end with a critical discussion on the opportunities and challenges offered by multiscale modeling and information transfer between scales to study amorphous plasticity.

(Some figures may appear in colour only in the online journal)

1. Introduction

Amorphous solids, or glasses, are not meant to deform. We all know that if we try to deform a piece of window panel, a compact disk or a sugar glass candy, the result is always the same: the glass is initially hard, deforms very little but breaks as soon as it starts to deform plastically. In mechanical terms, amorphous solids have a high strength and a low ductility. These traits also apply to the recently developed metallic glasses [13, 101, 112, 120, 217, 287] while their crystalline counterparts are known for exactly the opposite: low elastic limit and large deformation before failure. The low ductility of glasses is due to the localization of the plastic deformation in thin shear bands where local heating leads to decohesion and catastrophic

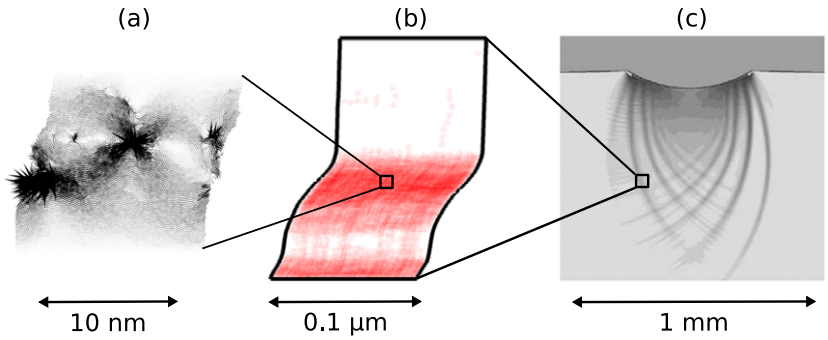

Figure 1. Illustration of a multiscale linking approach. The actual simulations were performed independently. In (*a*), atomic-scale simulations show localized atomic rearrangements, called shear transformations. Reproduced with permission from Springer Science + Business Media: Tanguy A *et al* 2006 *Eur. Phys. J.* E **20** 355. The energy of shear transformations is used in (*b*) to perform kinetic Monte Carlo simulations (the actual scale of the simulation cell is smaller than written here, 50 nm). Reproduced with permission from Homer E R and Schuh C A 2009 *Acta Mater.* **57** 2823. Copyright with permission from Elsevier. In (*c*), a micromechanical constitutive law is used to simulate indentation with the finite-element method. Reproduced with permission from Su C and Anand L 2006 *Acta Mater.* **54** 179. Copyright with permission from Elsevier.

failure [153]. Understanding and thus controlling shear band formation is the main challenge that has so far limited the use of glasses as structural materials [218].

Shear band formation is a typical multiscale phenomenon that occurs over three main length and time scales illustrated in figure 1. The elementary plastic events are atomic rearrangements called shear transformations (STs) [10, 11] that occur at the atomic scale and are localized both in space, involving only a few tens of atoms, and time, spanning a few picoseconds. At the micrometer scale, STs organize to form shear bands that appear within a few milliseconds and have a width on the order of a tenth of a micrometer [218]. Finally, at the macroscopic scale, depending on the loading condition, either a single shear band forms as in tension test, or several shear bands form and interact, in case of confined plasticity as in indentation tests [246].

The study of plasticity in amorphous solids has significantly benefited from computer simulations; probably more than crystalline solids, because of the lack of an experimental device able to identify plastic events in glasses, in the way electron microscopy images dislocations in crystals. Also the intrinsic brittleness of glasses at large scales forbids the use of standard mechanical tests. STs have been extensively studied using atomic-scale simulations (for a recent review, see [81]). At the micrometer scale, rate-and-state models (for recent reviews, see [19, 79]) based on the elastic interaction between STs have been used to study ST organization and its relation to shear banding. At the macroscopic scale, the finite-element method (FEM) has been used to simulate indentation [128, 246] and finite differences to study necking [72]. We stress that the above studies were carried out independently, while in a multiscale approach, we wish to tie them together in order to exchange information between scales. Multiscale modeling has been successfully applied to crystalline plasticity, with two main types of approaches. The first is a coupling approach where several simulations at different scales are performed simultaneously in a single computation framework, such as the quasicontinuum method that couples atomistic and finite-element simulations [176, 195, 223]. The second possibility is a linking approach where simulations at different scales are done sequentially and the results obtained at one scale are modeled in the form of local rules or phenomenological parameters used as input in the simulation at the scale above. As an

example, the linking approach has been applied to study the formation of shear bands in irradiated metals [182]. It is worth mentioning here that the development of dislocation dynamics [35, 59, 60, 156] at an intermediate (meso) scale between atomistic simulations and FE simulations has been a major step forward in the development of such multiscaling strategies.

Similar multiscale approaches would significantly benefit the study of amorphous solid mechanics. They have not yet been attempted, probably because our understanding of plasticity in amorphous solids is far less advanced than in crystals. In glasses, several very fundamental questions, starting at the atomic scale, should be answered before multiscale modeling can be performed.

(i) At the atomic scale, what triggers a ST? Since glasses are disordered and contain large fluctuations in local structure, density and composition, flow defects equivalent to dislocations in crystals have not yet been identified; only flow events or plastic rearrangements have so far been observed. The question is then if there is a way to identify regions prone to plastic rearrangement?
(ii) Still at the atomic-scale, what is the role of temperature on plastic events? Plastic activity has been compared with an effective temperature, but what is the interplay between effective and real temperatures?
(iii) STs produce elastic stresses and strains through which they interact with one another. But how does disorder interfere with elasticity?

Answering those questions would lead to the development of an equivalent of the dislocation theory of crystalline plasticity [105]. Multiscale modeling would then serve to answer equally fundamental questions at the micrometer and macroscopic scales:

(i) At the micrometer scale, how do shear bands arise from the interplay between ST interactions, local softening or hardening, and disorder in the glass structure and dynamics?
(ii) What happens during the millisecond or so before a shear band nucleates?
(iii) At the macroscopic scale, how are shear bands sensitive to the loading condition and how do they interact with one another?

The underlying issue behind the above questions is whether or not the state of a glass can be described by a finite set of internal variables, and whether or not the evolution of these internal variables can be tied to the loading history of the glass in order to describe the evolution of the glass state under deformation and its influence on the mechanical response. In a linking approach, the internal variables can then be used at the micrometer-scale in rate-and-state models to determine constitutive laws used in FEM at the macroscopic scale. This multiscale approach would be the equivalent of the dislocation density-based crystal plasticity theories that have proved very efficient in modeling plastic deformation in metals and alloys [60, 156].

Several reviews have been published recently on the mechanical behavior of glasses (see Schuh *et al* [218] for experiments, Falk and Maloney [81], Barrat and Lemaître [19] for simulations and modeling, and Falk and Langer for STZ theories [79]). In this paper, we focus on the multiscale modeling aspect of the study of glasses and associated challenges, with a particular attention to plasticity. To review the numerical simulation methods at the different length scale and time scale relevant for multiscale modeling, we start at the atomistic scale (sections 2 and 3), then address the mesoscopic scale (section 4) and finish with the macroscopic scale (section 5). At each scale, we emphasize the main specificities, successes and limitations of the different numerical techniques used to model glasses. We finally discuss opportunities and challenges offered by a multiscale linking approach to the study of plasticity in glasses (section 6).

2. Atomic-scale dynamics in the absence of deformation

The dynamics of disordered solids and liquids at the atomic-scale is highly complex and is the subject of a very vast and ever growing literature that cannot be reviewed exhaustively. We will focus here on numerical studies by means of molecular dynamics (MD) and statics simulations, and we adopt a specific angle of approach with the help of the *potential energy landscape* (PEL) picture. We start by presenting the elementary ingredients of atomistic simulations. We then review studies of the dynamics of liquids when cooled down to the glassy state.

2.1. Practicalities

Choice of interatomic potential. Accurately representing atomic bonding requires in principle electronic structure based methods, such as the density functional theory or self-consistent field calculations [264]. Electronic structure calculations have been applied to simulate liquids and glasses, but the tradeoff for increased accuracy is a decrease in system size (a few hundred atoms) and simulated time (a few picoseconds). Monoatomic systems (for example [20, 87, 117]), silica glasses (for example [114, 264]) and metal alloys (for example [88, 94, 127, 222]) have been simulated but semi-empirical potentials have also been used to access larger systems during longer times. For metallic alloys for example, the embedded atom method (EAM) formalism has been employed, in particular to model CuZr [68, 169, 170], CuZrAl [43] and CuMg [15] alloys. For liquid and glassy silica and silicon, several empirical potentials have been adjusted in order to fit, with a minimum number of parameters, *ab initio* cohesive energy data [20, 264] and experimental characteristics such as the melting temperature, short-range order, diffusive motion, some characteristic vibrational frequencies and elastic moduli [21, 37, 109, 114, 115, 244, 259, 267]. In the case of silicon, the difficulty is to find an empirical potential able to describe the profound structural breakdown that occurs upon melting, with an experimental average coordination of 4.0 in the solid phase (tetrahedral order due to sp3 covalent bonding in the crystal as well as in the amorphous phase) and of 6.4 in the liquid state [259]. Since the interatomic potentials depend on the full atomic configuration, they can be decomposed into two-, three-body potentials and above. The three-body potential serves to stabilize the ideal local bond angle, as in the famous Stillinger–Weber empirical potential [244], expressed as

$$V(1,\ldots,N) = \sum_{i<j} v_2(i,j) + \sum_{i<j<k} v_3(i,j,k) \tag{1}$$

with

$$v_2(i,j) = \epsilon.A.(Br_{ij}^{-p} - r_{ij}^{-q}) \exp[(r_{ij}-a)^{-1}],\ \mathrm{r}_{ij} < a \quad \text{and =0 elsewhere} \tag{2}$$

and

$$v_3(i,j,k) = h(r_{ij}, r_{ik}, \theta_{jik}) + h(r_{ji}, r_{jk}, \theta_{ijk}) + h(r_{ki}, r_{kj}, \theta_{ikj}) \tag{3}$$

with

$$h(r_{ij}, r_{ik}, \theta_{jik}) = \epsilon\lambda \exp[\gamma(r_{ij}-a)^{-1} + \gamma(r_{ik}-a)^{-1}].(\cos\theta_{jik} + \tfrac{1}{3})^2, \tag{4}$$

where r_{ij} is the bond length between atoms i and j and θ_{ijk} is the angle between the bonds ji and jk. The experimental pair correlation, however, is better reproduced with more complex environment-dependent potentials, such as Tersoff potential [259] or EDIP [21]. The latter is also able to represent the covalent-to-metallic transition through a parameter depending on the local coordination and describing the angular stiffness of the bond. These different empirical potentials have been tested on the nonlinear mechanical response of samples submitted to a

Table 1. Parameters of three common binary Lennard-Jones potentials. The cut-off radius R_C is expressed in units of the corresponding σ_{ij}. C_A and C_B are the concentrations of the two species.

	ϵ_{AA}	ϵ_{BB}	ϵ_{AB}	σ_{AA}	σ_{BB}	σ_{AB}	R_C	C_A	C_B
Kob-Andersen [131]	1	0.5	1.5	1	0.88	0.8	2.5	0.8	0.2
Wahnström [276]	1	1	1	1	$\frac{5}{6}$	$\frac{11}{12}$	2.5	0.5	0.5
Lançon *et al* [140]	0.5	0.5	1	$2\sin(\frac{\pi}{10})$	$2\sin(\frac{\pi}{5})$	1	5	0.45	0.55

large shear [91] or crack propagation [98]. In the case of silica, the ionic character of the bond is usually described through a two-body potential with partial charges [37, 171, 267], while the covalent character implies a three-body term [109]. Surprisingly enough, the local tetrahedral structure of SiO_2 is well described by a simple two-body potential with different charges on Si and O, even with a small cut-off of the interaction range [37].

In the field of liquids and glasses, most studies have aimed at understanding generic properties and in consequence have used the simplest possible phenomenological potentials. For example, most numerical works employed a binary Lennard-Jones (LJ) potential, an additive pairwise potential that physically represents noble gasses (Ar, Kr, Xe) with van der Waals interactions. Its expression is

$$v_2(i,j) = 4\epsilon_{ij}\left[\left(\frac{\sigma_{ij}}{r_{ij}}\right)^{12} - \left(\frac{\sigma_{ij}}{r_{ij}}\right)^{6}\right] + B_{ij}r_{ij} + C_{ij}. \tag{5}$$

The linear function in the rhs is added to the original potential to ensure that the potential and interaction force go smoothly to zero at the cut-off radius. Sometimes, quadratic functions are used to additionally ensure smoothness of the second derivative. Table 1 summarizes the parameters of the 3 most common LJ potentials used in the literature.

By far, the most widely used potential was developed by Kob and Andersen [131] to reproduce the properties of $Ni_{80}P_{20}$. One should note that this potential is highly non-additive, that is $\sigma_{AB} \neq (\sigma_{AA} + \sigma_{BB})/2$ and $\epsilon_{AB} \neq (\epsilon_{AA} + \epsilon_{BB})/2$. Non-additivity is present in Lançon *et al* potential [140]. The latter potential has been used in 2 dimensions because of its quasicrystalline ground state. By way of contrast, the second most common potential, developed by Wahnström [276], is strictly additive. Thus, good glass-formability does not necessarily require non-additivity of the potential. Generalized LJ potentials have also been employed, for instance to simulate CuZr metallic glasses [134, 135] with exponents 4–8 instead of 6–12, which proved better suited to represent metallic bonding.

Choice of boundary conditions. The most popular boundary conditions are periodic. In most cases, deformations are applied using strain-controlled boundary conditions implemented by changing the simulation cell dimensions and shape: uniaxial traction and compression (with a pressure control in the transverse directions to maintain zero pressure transversally), pure and simple shear. In latter case, Lees-Edwards shifted periodic boundary conditions are applied, whereby periodicity across two opposite faces of the simulation cell is shifted with respect to each other in the shear direction (which is equivalent to applying periodic boundary conditions in a non-orthonormal cell [2]). Fixed and free boundary conditions have also been used.

The choice of boundary conditions is not inconsequential since fixed boundaries favor localization of the deformation in simple shear parallel to the boundary and impede localization in the transverse directions [273]. Similarly, uniaxial traction with free surfaces in the transverse directions also favor shear localization compared with simple shear with periodic boundary conditions [42].

MD versus athermal quasistatic simulations. The first step of an atomistic simulation of a glass is to produce an initial configuration by quenching a liquid using MD. The procedure involves first equilibrating the liquid at an elevated temperature (typically several 1000 K) and then progressively decreasing the temperature below the glass transition at either fixed volume or fixed pressure. The main limitation of MD simulations is that the time scale is very limited, typically a few tens of nanoseconds. As a consequence, MD quench rates are on the order of $1000\,\mathrm{K}/10^{-8}$ s, i.e. 10^{10} to $10^{12}\,\mathrm{K\,s^{-1}}$, which is enormously high compared with experimental quench rates that are rather on the order of $10^{6}\,\mathrm{K\,s^{-1}}$ for the first synthesized metallic glasses [130] to $0.1\,\mathrm{K\,s^{-1}}$ for the most recent bulk metallic glasses [120]. As a result, simulated glasses are inevitably far less relaxed than experimental glasses, with consequences on their propensity to form shear bands that will become apparent later in the text. Also, when simulating the deformation of glasses using MD, one wishes to reach a strain of order 1 in the time scale of the simulation, resulting in typical strain rates of $\dot{\gamma} = 1/10^{-8} = 10^{8}\,\mathrm{s^{-1}}$ compared with typically $10^{-3}\,\mathrm{s^{-1}}$ experimentally. In order to avoid this discrepancy, one option is to apply athermal quasistatic (AQS) deformations [157, 161, 162]. The system is then sheared in small increments followed by energy minimizations at fixed applied strain. This protocol corresponds to the limit $T \to 0$, since the energy minimizations remove all thermal activation, and $\dot{\gamma} \to 0$, since the system is allowed to fully relax to a new energy minimum before a new strain increment is applied [157].

The physical situation associated with the AQS procedure involves two time scales characteristic of the dynamics of glassy materials [25]. The first time scale, τ_{diss}, is the time it takes for a localized energy input to spread over the whole system and be dissipated as heat. The corresponding mechanisms can be viscous (in a soft material) or associated with phonon propagation or electron transfers (in a metallic glass). AQS deformation corresponds to a typical time between consecutive strain increments much larger than τ_{diss}, that is $\dot{\gamma} \ll \delta\gamma/\tau_{\mathrm{diss}}$, where $\delta\gamma$ is the elementary strain increment. A second, much longer time scale is the structural relaxation time of the system, τ_{α}, associated with spontaneous aging processes that take place at finite temperature in the absence of external drive. By quenching after every displacement step, any such processes are suppressed and the time elapsed between consecutive increments is thus far smaller than τ_{α}, i.e. $\dot{\gamma} \gg \delta\gamma/\tau_{\alpha}$. Here, $\delta\gamma$, the elementary strain step, is chosen small enough to ensure that the system remains in its initial basin when starting from any equilibrium configuration ($\delta\gamma$ depends on the system size, probably logarithmically [147] and is on the order of 10^{-5} for $L = 100$ in LJ units in 2 and 3 dimensions [148]). This picture is of course oversimplified. Relaxations in glasses are in general stretched [25], meaning that relaxation processes take place over a broad spectrum of time scales and the AQS approach ignores the fast wing of the relaxation spectrum. Another drawback of the AQS approach is that it ignores thermal effects that are unavoidable in experiments. The coupling between temperature and strain rate is highly non-trivial and progress in this area will be discussed in section 3.2. The first steps toward using accelerated dynamics has been taken [136, 204] in order to access slow dynamics at the atomic scale, but such simulations are difficult because of the complexity of the configurational paths available to disordered systems.

2.2. Cooling a liquid

Understanding the glass transition and the associated dramatic slowing down and increasing heterogeneity of the liquid dynamics is a topic of intense research (for reviews, see, for example, [24, 54, 73, 104, 253, 258]). This field has significantly benefited from the recognition that the dynamics of a cooling liquid is intimately related to the topography of its underlying PEL [279].

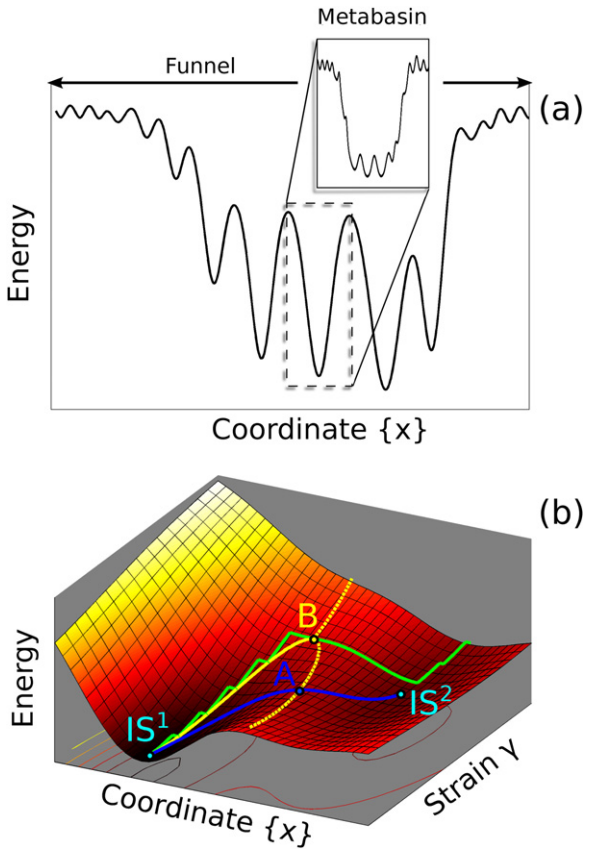

Figure 2. Schematic illustration of PELs in (*a*) two and (*b*) three dimensions. See text for details.

What is the PEL? An atomic configuration is represented in configuration space by its position vector, R^{3N}, a $3N$-dimensional vector for a system of N particles in 3 dimensions. The potential energy of the system, $V(R^{3N})$, is then a $3N$-dimensional surface, termed the PEL, in the $(3N+1)$-dimensional space composed of configuration space and the energy axis [92, 277]. It is important to note that the PEL depends only on the interatomic potential and the boundary conditions. Thus, for a given potential and given boundary conditions, all configurations of a system, whether they are crystalline, amorphous or liquid, share the same PEL; only the region of configuration space visited by the system depends on the state of the system.

As sketched in figure 2 in two and three dimensions, the PEL contains extrema, or *stationary points*, which may be local maxima, local minima called *inherent structures* (ISs) [243] (IS^1 and IS^2 in figure 2(*b*)) and saddle points (*A* in figure 2(*b*)). Stationary points are classified by their index, which is the number of negative eigenvalues of the Hessian matrix (matrix of second derivatives of the potential energy) computed at the stationary point [277]. The PEL can be partitioned into valleys, or *basins*, that surround each local minima [242, 243]. More precisely, the basin (of attraction) of an IS is the region of configuration space where all configurations converge to the IS upon steepest-descent energy minimization. In figure 2(*b*), the basins of IS^1 and IS^2 are delimited by the yellow dashed line. Alternatively, the PEL can be partitioned using the basins of attraction of all stationary points and not only local minima by minimizing the objective function $\frac{1}{2}|\nabla V(R^{3N})|^2$ rather than the potential energy [6], although

one has to be careful that the objective function has more minima than stationary points on the PEL [67].

The number of stationary points increases roughly as an exponential function of the number of atoms in the system [104, 243]. It is therefore impossible in practice to list exhaustively all stationary points in a PEL, except for very small systems (containing typically 32 atoms or less [7, 103]). On the other hand, statistical information, such as distributions of activation energies, can be computed accurately on tractable samples containing typically a few thousand events [203].

Hierarchical structure of the PEL. The relation between liquid dynamics and PEL was probed by means of MD simulations (mostly binary LJ liquids modeled using Kob and Andersen potential) with regular energy minimizations in order to determine the succession of ISs visited by the liquid during its time trajectory [122, 214, 215, 243]. The mode-coupling temperature (T_C) [93] plays the role of reference temperature for the dynamics of liquids at the atomic scale. Examples of quenches are shown in figure 3(*a*) using the Wahnström LJ potential in conditions where $T_C \sim 0.6$ [215, 216]. Three regimes were identified [214]. At high temperature, above about $1.5T_C$, the system is fully liquid and the kinetic energy is high enough that the system hardly feels the underlying PEL.

At lower temperatures, the system becomes supercooled and enters the so-called *landscape influenced regime*. Between $1.5T_C$ and T_C, the liquid gets progressively trapped in basins of decreasing energy. If the quench rate is low enough, the system is at equilibrium at all temperature above T_C and the IS energy follows an equilibrium function of temperature [133, 138, 215]. A decoupling progressively develops between the rapid motion of the supercooled liquid inside a basin (intrabasin vibration) and the infrequent transitions to a new basin (interbasin hopping) [220]. Vibrations are, however, of large amplitude and the system spends most of its time in the basins of attraction of saddle points, i.e. stationary points with index 1 and above [6, 30]. A well-defined relation was found between the average stationary point index and the temperature or potential energy [6, 30] with the average index vanishing precisely at T_C. The progressive trapping of the system implies that the PEL has a multifunnel structure [277, 278] where, as illustrated in figure 2(*a*), the basins are organized in pockets of ISs with increasing energy barriers for decreasing IS energy.

Funnels have a hierarchical structure. On short time scales, the system undergoes a back and forth motion between a limited number of basins forming a cluster, also called a *metabasin* [242], while on longer time scales, the system performs an irreversible Brownian diffusion between metabasins [31, 58, 62, 63]. The above dynamics implies that, as illustrated in figure 2(*a*), metabasins are composed of basins connected by low-energy saddle points, while different metabasins are separated by higher energy barriers. Moreover, some metabasins are visited quickly whereas others are very long-lived [64]. The overall structure of the PEL is therefore a multifunnel rough landscape [278] with a hierarchy of energy barriers connecting basins and metabasins. Trapping of the supercooled liquid in this maze of interconnected basins and the multistep hopping process between long-lived metabasins was put forward to explain the rapid slowing down and stretched exponential relaxations of liquids across the glass transition [64, 104].

Below T_C, the system falls out of equilibrium. The system enters the glassy state, or *landscape dominated regime* [216], which is the true thermally activated regime where the system spends most time vibrating near local minima and undergoes rare and thermally activated transitions between ISs. As seen in figure 3(*a*), the energy of the final IS decreases with decreasing quench rate, meaning that the glass is better relaxed. This is a consequence of the funnel structure of the PEL where decreasing quench rates give more time to the

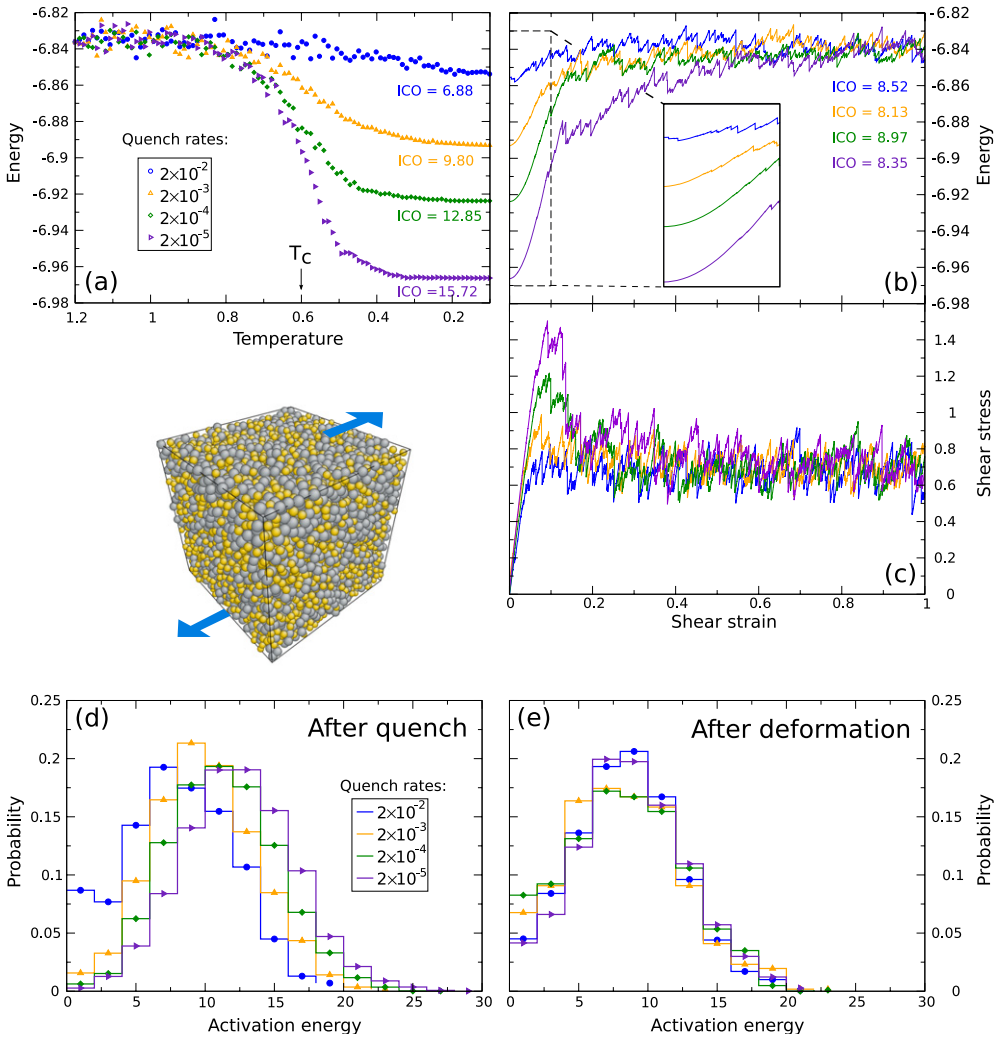

Figure 3. Influence of quench rate on the cooling and deformation of glasses: (*a*) inherent structure energy during quenches at different rates, (*b*) energy–strain curve and (*c*) shear stress–shear strain curve during simple shear deformation, (*d*) distribution of activation energies around as-quenched configurations, (*e*) same distributions after plastic deformation. The system of 10 000 atoms of a 50 : 50 binary mixture of LJ atoms modeled with Wahnström potential, in a cubic cell of length 19.74 σ_{AA}. Quenches were performed at fixed volume after equilibration at $k_{\mathrm{B}}T = 1.2\epsilon_{AA}$ for 5×10^3 t_0. Quench rates are expressed in units of $\epsilon_{AA}/k_{\mathrm{B}}t_0$. The fraction ICO of icosahedron-centered atoms is computed using a Voronoi tessellation. In (*b*) and (*c*), shear deformation is applied quasistatically with a strain increment of 10^{-4} followed by energy minimization using Lees-Edwards boundary conditions. Activation energy distributions in (*d*) and (*e*) are obtained using the activation–relaxation technique with samples containing a minimum of 1000 saddles.

system to explore lower regions of the funnel before being trapped. When the temperature is lowered below T_{C}, the waiting time between transitions rapidly exceeds MD time scales and the PEL can no longer be probed by direct MD simulations. In this regime, saddle-point search methods can be used to identify activated states on a PEL. Examples of distributions of the activation energies of transition states (saddle points of index 1) around the final

ISs obtained after the above quenches are shown in figure 3(*d*). These distributions were obtained using the activation–relaxation technique (ART) [36, 159, 204]. Distributions of activation energies have a characteristic shape with a broad energy spectrum and a maximum, i.e. a most likely activation energy. Similar distributions were obtained in LJ glasses [6, 173, 204] as well as amorphous silicon [266]. Their exponential tail agrees with the master-equation approach developed by Dyre [71] in the case of rapidly quenched glasses. Also, the density of low activation saddles (below typically $5\epsilon_{AA}$ for this system) decreases for configurations relaxed more slowly. The latter configurations are therefore more stable, both thermodynamically, because they have a lower energy, and kinetically, because they are surrounded by higher activation energies. In experimental glasses that are quenched much more slowly than in simulations, we expect activation energies to be shifted toward higher energies without low activation energies, although a quantitative study of this dependence remains to be done.

Below T_C, glasses are not in thermal equilibrium and evolve toward deeper regions of the PEL. This relaxation process is slow and referred to as structural relaxation or *physical aging* [245, 265]. Two relaxation time scales have been identified, β-relaxations on short time scales and α-relaxations on longer time scales [119]. In relation with the PEL picture, Stillinger [242] hypothesized that β-relaxations are transitions inside a given metabasin while α-relaxations would be transitions between metabasins. MD simulations confirmed the first hypothesis but showed that the second is only partly true. A β-relaxation is a transition inside a given metabasin, termed *nondiffusive* by Middleton and Wales [173] because it corresponds to a slight repositioning of atoms inside their shell of nearest neighbors (*cage effect*). By way of contrast, transitions between metabasins involve bond switching and correspond to localized rearrangements in the form of string-like sequences of displacements whose size ($\sim$10 atoms) increases as the temperature decreases toward T_C [65, 66, 132, 216, 241]. One such dynamical heterogeneity is, however, not an α-relaxation in itself because it occurs on a time scale of the order of $1/10$ to $1/5$ of the α-relaxation time scale [8]. An α-relaxation is therefore made of 5 to 10 metabasin transitions. It remains localized in the microstructure but involves more atoms than string-like events ($\sim$40 atoms), is more globular and was termed *democratic* [8]. Dynamical heterogeneities have been shown correlated with both localized soft modes [280] and fluctuations of static structural order [126, 253].

Atomic-scale glass structure. Although glasses are disordered at long range, they exhibit short- and medium-range orders. There exists no general theory to predict the packing in a given glass but short- and medium-range orders have been studied in a number of metallic glasses using a combination of experiments and simulations (see, for example, [41, 68, 96, 134, 189, 222]). It was shown that solute atoms tend to remain separated from one another and their shell of first neighbors tends to form simple polyhedra. In several binary glasses, and in particular CuZr metallic glasses, the most abundant polyhedra are Cu-centered icosahedra, therefore atoms with a local fivefold atomic environment [42, 122, 192]. Moreover, it was shown that in this system, the short-range order can be characterized by the density of these icosahedra, which is strongly correlated with the level of relaxation of the glass. In particular, Cheng *et al* [42] showed that the density of Cu-centered icosahedra increases rapidly in the landscape influenced regime and reaches a low-temperature value that increases with decreasing quench rate, i.e. increasing levels of relaxation. This result is shown in figure 3(*a*) by the increase of the fraction of icosahedron-centered atoms (ICO) with decreasing quench rate. Icosahedron-centered atoms are clear markers of the level of relaxation of a glass but they concern unfortunately only a certain class of metallic glasses. They are relevant for Wahnström potential [46, 190] but are not the most frequent local environment in monoatomic glasses and

the addition of a three-body term to the interatomic potential changes drastically the atomic structure and ability to crystallize [86, 177, 229, 252].

3. Atomic-scale deformation of glasses

3.1. AQS deformation

PEL and AQS deformation. The PEL picture also proved useful to rationalize the behavior of glasses under deformation, as first demonstrated by Malandro and Lacks [137, 157, 158]. The picture is clearest during AQS deformation where the glass evolution is exclusively strain activated and when rigid boundary conditions are used. In this case, a shear strain is applied by rigidly moving in opposite directions two slabs of atoms on opposite faces of the simulation cell. The PEL is then unchanged because the potential energy function is unchanged (the situation is different when stresses are applied because the PEL is then tilted by the work of the applied stress [14]). The effect of an applied strain is then to force the system to visit new regions of the PEL. More precisely, adding a strain increment to a simulation cell amounts to moving the system in a given direction of configuration space, which we call the strain vector γ. The PEL may thus be represented in three dimensions as in figure 2(*b*), with the strain vector γ isolated from the other dimensions of configuration space, noted $\{x\}$. A possible path during AQS deformation is shown in green in figure 2(*b*). Initially, the as-quenched glass is in an IS, noted IS^1, at the bottom of an energy basin. The strain increments push the system away from this initial configuration. After each strain increment, the energy is minimized at fixed strain, i.e. minimized in the hyperplane perpendicular to the strain vector. The system then relaxes to the nearest local minimum in the hyperplane, which lies on the branch of stable equilibrium at the bottom of the basin, shown as a yellow solid line in figure 2(*b*). During the first few strain increments, the system remains in the initial basin and the deformation is purely elastic and reversible; if the strain is removed, the system relaxes back along the stable branch down to IS^1. The extension of this region of strict reversibility increases with decreasing system size and increasing level of relaxation of the quenched glass (see figure 3(*b*)).

With increasing strain, the system reaches the edge of the initial basin, noted *B* in figure 2(*b*), a position of instability on the PEL where the stable branch at the bottom of the basin (yellow solid line) meets the unstable branch on the border of the basin (yellow dashed line). At this point, one eigenvalue of the Hessian matrix in the hyperplane of constant strain vanishes. Such instability is called a saddle-node or a fold bifurcation [95]. Near the instability, glasses have a universal behavior [40, 124, 161]: the vanishing eigenvalue and energy barrier between stable and unstable positions go to zero as $(\gamma_C - \gamma)^{1/2}$ and $(\gamma_C - \gamma)^{3/2}$, respectively, where γ_C is the strain at the bifurcation. The subsequent energy minimization takes the system into a new basin, centered on IS^2 in figure 2(*b*). During the relaxation, the system is out-of-equilibrium and its trajectory depends on the energy minimization algorithm used. Across the transition, the position of the system on the PEL, as well as its energy and stress are discontinuous. The transition is irreversible because if the strain is decreased, the system remains in the new basin. Such transitions are the elementary events that produce dissipation and plastic strain during the deformation process. During a AQS process the kinetic energy produced by the elementary events is assumed to be very efficiently dissipated in order to relax in the next visited basin.

Shear transformations and avalanches. Figures 3(*b*) and (*c*) show examples of energy–strain and stress–strain curves during simple shear deformation of the quenched glasses obtained in figure 3(*a*). As expected from the above discussion, the curves are made of continuous

elastic segments intersected by plastic events where stress and energy are discontinuous [157, 158, 161, 256]. The deformation starts with a regime where the stress increases linearly with strain and the energy increases quadratically. This regime is larger than the region of strict reversibility mentioned above and contains small plastic events as evidenced by the discontinuities in the inset of figure 3(*b*). The latter correspond to localized rearrangements in the microstructure [55, 158, 161, 168, 256]. They are the STs proposed by Argon [10, 11] as elementary plastic events in amorphous solids. An example in two dimensions is shown in figure 1(*a*). The rearrangement is composed of two regions: a plastic core region where atomic bonds are cut and reformed and a surrounding elastic region, which responds elastically to the plastic rearrangement. In figure 1(*a*), mainly the elastic field is visible with a quadrupolar symmetry [161, 256], characteristic of an Eshelby field (see section 4.1 and equation (20)). This field was shown to scale with the eigenmode whose eigenvalue vanishes at the instability [146, 160, 257]. Evaluating the size of a ST requires separating the plastic region, which is the true ST zone, from the elastic surrounding. Such separation is not straightforward, but usual estimates are 20 atoms in two dimensions [256] and 100 in three dimensions [288]. The corresponding local strain is about 0.1, which satisfies the Lindemann instability criterion with a relative displacement of the particles of a tenth of the interatomic distance [256, 262].

As strain increases, the system reaches its true elastic limit where plastic flow starts. Irreversible events are then dominated by large rearrangements that span the entire simulation cell [16, 161, 256]. Careful analysis of energy minimizations during such rearrangements [57, 161] showed that, although the system is out-of-equilibrium and does not cross any equilibrium configuration (otherwise the energy minimization would stop), the path can be decomposed into a succession of localized unstable STs that trigger each other through their elastic strain and stress fields. The latter thus play the role in AQS simulations of a mechanical noise that can push local regions beyond their stability limit leading to out-of-equilibrium cascades of STs [146]. Avalanches do not necessarily lead to persistent shear bands since, as discussed below, depending on the boundary conditions and on the interatomic interactions, the cumulative deformation can remain homogeneous in the avalanche regime for at least several 100% strain.

Relating the elastic limit to the PEL picture, Harmon *et al* [97] proposed that the elastic limit occurs when the glass leaves its initial metabasin while STs are transitions between basins inside a given metabasin. However, from the PEL analysis of supercooled liquids presented in section 2.2, we know that transitions inside a given metabasin correspond to small atomic adjustments that retain the nearest-neighbor shell while transitions between metabasins involve bond switching, as in STs. STs are thus elementary transitions between metabasins and are analogous to string-like events in supercooled liquids, while avalanches, made of a succession of STs, correspond to a transition over several metabasins and would be analogous to α-relaxations.

A question of prime importance then arises: can we predict the location of the next ST? Or said differently, is there a structural signature that indicates a region prone to plastic rearrangements, also called *weak region*, or *ST zone* [78]? Historically, the first proposed criterion was based on local atomic stresses. Srolovitz *et al* [237, 238] in their early simulations of metallic glass plasticity identified three types of structural defects: atoms with high atomic tensile or compressive stress (n- and p-type defects, respectively) and atoms with high atomic shear stress (τ-defects). Plastic rearrangements upon shear deformation were shown uncorrelated with n- and p-defects but a correlation was found with τ-defects. A more recent study in a 2D sheared LJ glass [262] showed, however, that the increase in local shear stress occurs only right before the plastic event, with an average relative increase of the local shear stress of only about 3%, as shown in figure 4(*f*), very difficult to identify experimentally.

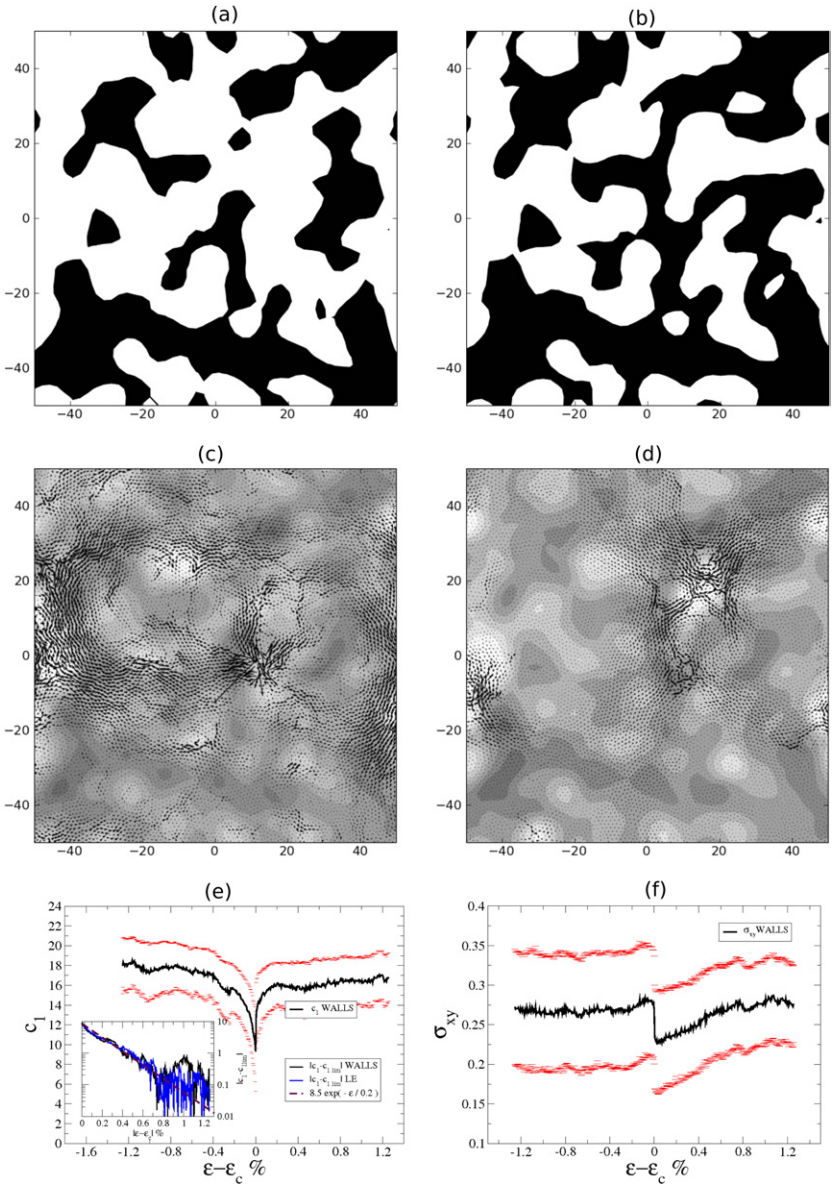

Figure 4. Elasticity map and nonaffine displacements in a 2D shear LJ glass. In (*a*) and (*b*), the shear modulus is divided into rigid ($c_1 > \overline{c_1}$, black) and soft ($c_1 < \overline{c_1}$, white) zones for 2 strains: (*a*) 2.5 %, (*b*) 2.55%. In (*c*) and (*d*), nonaffine displacements are superimposed on the local map of shear modulus for the same configurations as in (*a*) (for (*c*)) and (*b*) (for (*d*)). In (*c*), the nonaffine field is multiplied by 300 to illustrate the very strong correlation between elastic nonaffine field and elasticity map. In (*e*) and (*f*), are shown the variations of c_1 and shear stress, averaged over plastic events. Reproduced with permission from Tsamados M *et al* 2009 *Phys. Rev.* E **80** 026112. Copyright (2009) by the American Physical Society.

Moreover, this small change is smaller than local-stress fluctuations, and is not visible in the distribution of shear stresses for atoms in regions just about to rearrange plastically, which is the same as the overall distribution computed over all atoms [263]. A criterion based on

local stresses therefore appears not adequate at small scales, even if a definite yield stress appears at large scales (see discussion in section 4.1). A more promising route concerns local elastic moduli. Tsamados *et al* [257, 262] computed the local elasticity tensor through a coarse-graining procedure in a 2D sheared LJ glass and proposed as order parameter the lowest eigenvalue of the local elasticity tensor, c_1. Strong elastic heterogeneities were found at the nanometer scale that decay for larger coarse-graining scale. The nanometer scale (between 5 and 20 σ_{AA}) appears the most appropriate scale to describe elastic heterogeneities, since linear elasticity appears to be valid at that scale, and local anisotropy and spatial heterogeneities are measurable. As illustrated in figures 4(*a*) and (*b*), the glass is composed at this scale of a rigid scaffolding (black regions where $c_1 > \overline{c_1}$, where $\overline{c_1}$ is the average order parameter) and soft zones (white regions where $c_1 < \overline{c_1}$). Note that rigid and soft zones are not fixed in the microstructure but evolve dynamically during the deformation (as seen by comparing figures 4(*a*) and (*b*)). Also, as shown in figures 4(*c*) and (*d*), a strong correlation was found between plastic activity and soft zones at the nanometer scale: c_1 vanishes locally prior to a plastic event, with a marked 37% exponential decay of its amplitude, over a characteristic strain range of 0.2%. Elastic constants being related to the Hessian matrix, this result shows that the global Hessian matrix, which has a vanishing eigenvalue at the plastic event, can be computed locally over finite-size regions with the same property: the local Hessian matrix has a vanishing eigenvalue in the region of plastic activity. But noticeably, the decay of the heterogeneous elastic constants measured on the local Hessian matrix [262], that is at the nanometer scale, appears far before ($\delta\gamma \approx 0.2\%$) the decay of the eigenvalues of the global Hessian (which occurs only within $10^{-3}\%$ of the transition [160] with possibly an influence of the simulation cell size). Prediction of plastic activity thus combines the local measurement (at the nanometer scale) of a global quantity (the coefficients of the Hessian matrix). The same result was obtained for dislocation nucleation in crystals [175]. However, as shown in figure 4(*e*), c_1 decreases only near the instability and the next plastic event cannot be predicted until the glass is brought close to the instability. The question of the existence of identifiable structural defects in metallic glasses is therefore still largely open. The situation is different in amorphous silicon where weak (or liquid-like) and strong (solid-like) regions can be identified by looking at their radial and angular distribution functions [56, 86, 252].

Influence of initial configuration. As seen in figures 3(*b*) and (*c*), plastic yielding strongly depends on the level of relaxation of the initial glass. Slowly quenched glasses that are more relaxed show a marked *upper yield point* followed by softening, while less-relaxed glasses have no upper yield point [43, 86, 224, 226, 265]. Also, the extension of the purely elastic regime increases strongly with the level of relaxation of the glass. After yielding, when simple shear is applied as in figure 3, the glass enters a steady-state regime, called a *flow state*, which is independent of the initial configuration in the sense that the energy, stress and fraction of icosahedron-centered atoms reach steady-state values independent of the initial configuration, as shown in figure 3(*b*). One may say that the glass has lost the memory of its initial configuration [265]. Persistent localization has been observed in this regime, but depends on the level of relaxation of the initial quenched glass, the boundary conditions as well as the interatomic potential. Persistent localization occurs mainly in slowly quenched glasses [224, 226] and is favored in simple shear by fixed boundaries [273] and in uniaxial straining by free surfaces [42, 43, 224, 226]. A strong three-body term in the interatomic potential also favors plastic localization, as well as a low pressure [86, 252]. Sampling of the PEL around deformed configurations taken from the flow state, as shown in figure 3(*e*), shows a marked increase in the density of low activation energies compared with the initial quenched glasses except for the most rapidly quenched glass [203, 204]. This effect has

also been measured experimentally [129]. Similarly, as seen in figure 3(*b*), the fraction of icosahedron-centered atoms decreases after deformation [1, 42], again with the exception of the most rapidly quenched glass, which was so far from equilibrium initially that it evolved toward a slightly more relaxed glass during deformation, a process called *overaging* [275].

3.2. Influence of temperature

Deformation acts in a way analogous to heating above T_C since it accelerates the dynamics of the glass and gives access to high-energy ISs that had become inaccessible below T_C. The glass microstructure evolution under deformation, or *rejuvenation* [28, 44, 245, 265, 275], has been opposed to *aging* because the deformation reverses the aging process by increasing the energy of the glass and decreasing its stability. Also, as seen in figure 3(*b*), the steady-state IS energy in deformation is the same as in the high-temperature liquid regime. Moreover, it is known experimentally that the thermal history (annealing) affects the structure of a glass through its density fluctuations at rest [53, 152]. This effect could be compared with the structural changes that occur when the system is submitted to a plastic deformation at a given strain rate. In addition, the plateau resulting from the cage effect [22], which arises in temporal correlation functions used to characterize the dynamics of glasses, disappears progressively with both an increasing shear rate and an increasing temperature. Finally, it is well-known experimentally that the viscosity of supercooled metallic liquids [125, 172, 200] or of oxide glasses [231] decreases as a function of both temperature or shear rate. There is therefore a strong interplay between temperature and strain rate. From a theoretical point of view, the effect of temperature has been taken into account in mean-field (MF) models of plasticity, where plastic events are triggered randomly by thermal fluctuations in specific distributions of energy barriers [100, 234, 235] or activated volumes [78]. Also in the rate-and-state models, an effective Vogel–Fulcher law has been used to describe both deformation induced disorder and annealing mechanisms [80]. In the numerical simulation of mechanically deformed systems at finite temperature, two main difficulties must be considered: first the competition at small scale between the mechanically driven dynamics and the local dynamics of the thermostat used to maintain the temperature, and second the necessity to identify very carefully the temperature domain studied, which is a function of the applied shear rate.

Influence of the thermostat. This first difficulty is inherent to all MD simulations. The latter consist of solving the discretized Newton's equations of motion with different constraints, such as constant total energy (microcanonical ensemble) or constant temperature (canonical ensemble). The temperature is defined by the equipartition theorem through the average fluctuation of particle velocities:

$$\left\langle \sum_{i=1}^{N} \frac{1}{2} m_i \delta v_i^2 \right\rangle = \frac{3}{2} N k_B T. \tag{6}$$

When a system is deformed plastically by MD, a thermostat must be used because the work produced by the plastic deformation is transformed into heat and the temperature will rise indefinitely. Interestingly, all thermostats involve characteristic time scales that depend on arbitrary parameters. For example, the simplest thermostats (Berendsen thermostat, rescaling of velocities) [85] preserve equation (6) with a characteristic time depending on the coupling coefficient to the heat bath for the Berendsen thermostat, and on the frequency of rescaling for the velocity rescaling. More elaborated thermostats, such as Langevin, Andersen or Nosé–Hoover thermostats, also involve characteristic times, related to the damping coefficient for

the Langevin thermostat, the probability of collision for the Andersen thermostat, and the dynamical coupling to fictive variables for the Nosé–Hoover thermostat.

These time scales are important because the dynamics of the thermostat can interfere with the driven dynamics of the system. For example, a very frequent rescaling of the velocities slows down the driven dynamics, while local heating can be unrealistically high in the opposite case. The thermostat parameters may be chosen on physical grounds if the dynamics of the dissipative processes acting in the system are known, but characterizing such processes is a major difficulty. As a result, MD simulations usually simply involve a spatially homogeneous velocity damping with an arbitrary intermediate value for the damping coefficient.

Temperature domains. A first attempt to bridge the gap between atomic-scale simulations and macroscopic descriptions is to try to identify different temperature ranges on physical bases. At the small scale, the thermal kinetic energy due to atomic displacements can be compared with the dissipative energy associated with different processes, and to the driving energy. Different temperature domains can thus be defined, with boundaries that depend on the applied strain rate. A first limiting case is the *athermal regime*, which may be defined [261] as the regime where the typical relative displacement between particles due to the external strain $a\dot{\gamma}t$ (where a is the interatomic distance, $\sim\sigma_{AA}$ for a LJ potential) is larger than the typical vibration of an atom due to its local thermal activation, $\sqrt{k_B T/K}$ with $K = m\omega_D^2$ and $t = 2\pi/\omega_D$, resulting in a condition on the temperature T:

$$T < \frac{4\pi^2 m a^2}{k_B}\dot{\gamma}^2, \qquad \text{or in LJ units: } T < 4\pi^2\dot{\gamma}^2. \tag{7}$$

This condition is very strict for a LJ glass ($T < 40\dot{\gamma}^2 \approx 4\times10^{-7}$ for $\dot{\gamma} = 10^{-4}$) but quite usual for a colloidal glass ($\dot{\gamma} > 10^{-6}\,\mathrm{s}^{-1}$ at $T = 300\,\mathrm{K}$ for millimetric beads with $m = 1g$). In this regime, which corresponds to $T \to 0$, Tsamados [261] checked the progressive convergence to the QS regime when $\dot{\gamma} \to 0$, as illustrated in figure 6(*a*). In the athermal regime, the rheological law for the flow stress follows a Herschel–Bulkley law [102]:

$$\sigma_0(\dot{\gamma}) = \sigma_{AQS} + A\dot{\gamma}^m, \tag{8}$$

where σ_{AQS} is the flow stress in AQS condition and $m = 0.4 \sim 0.5$, as shown in figure 6(*b*) [22, 144, 206, 261]. Similar behavior was also found experimentally in dense colloidal systems [45, 254].

Under deformation at finite temperature, the particles exhibit a thermal as well as a mechanically driven diffusion. Collective effects in atomic diffusion in glasses have been known for a long time [75]. In the AQS regime, numerical simulations showed that the particles display a diffusive behavior at large strains due only to the plastic rearrangements upon external driving [146, 256, 261] as shown in figure 5. In the athermal regime, the particles show first a ballistic motion followed by a diffusive behavior at longer time scales (see figure 6(*d*)) with a cross-over time that decreases for increasing shear rates $\dot{\gamma}$. Interestingly, as shown in figure 6(*d*), in the 2D LJ glass studied in [261], the diffusive coefficient, D_{eff}, defined as a function of the strain γ rather than time (to transpose easily the definition to the AQS regime) decreases with the shear rate as $D_{eff} \equiv \langle\Delta y^2\rangle/2\Delta\gamma \propto \dot{\gamma}^{-0.5}$ for large $\dot{\gamma}$, with a finite-size saturation at small $\dot{\gamma}$, i.e. in the AQS regime. This decrease of the diffusion coefficient can be compared with the decrease of the Lindemann relaxation time t_{MSD} defined by $< \langle\Delta y^2(t_{MSD})\rangle^{1/2} = 0.1a$, which corresponds to the typical time a particle needs to escape definitely from its initial cage (here through the plastic rearrangements due to the external driving) and is often associated with τ_α, the characteristic time for α-relaxation (see section 2.2). Of course, $t_{MSD} \sim \tau_\alpha \propto \dot{\gamma}^{-0.5}$ due to the $\dot{\gamma}$-dependence of D_{eff}. Also,

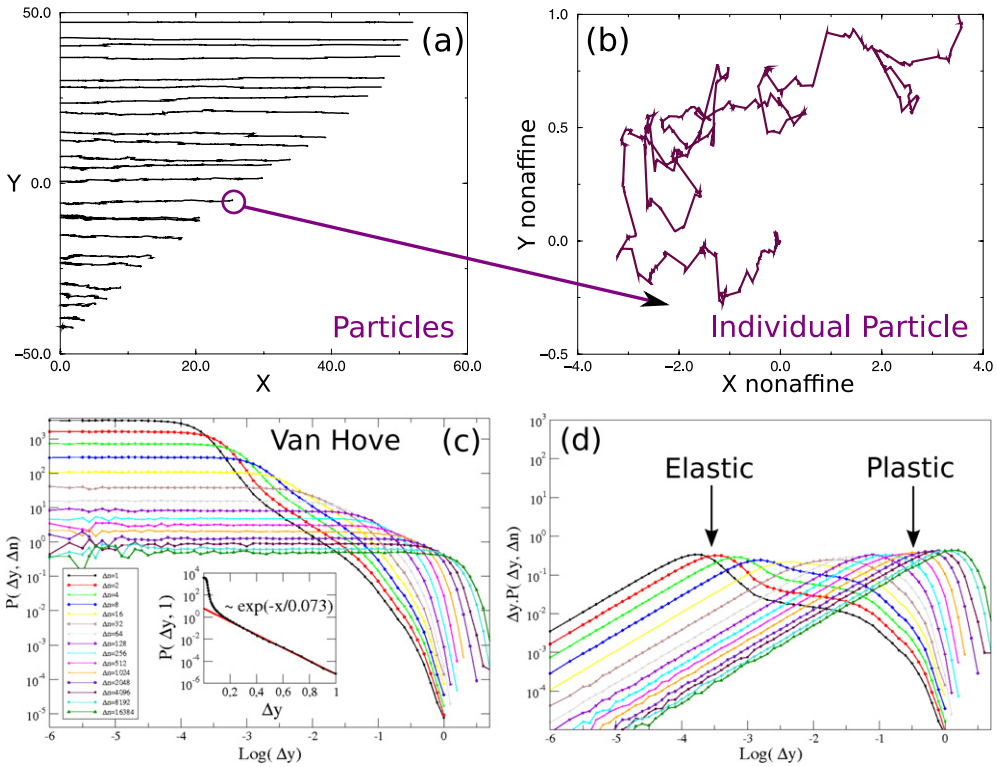

Figure 5. Stochastic analysis of the nonaffine part of the individual motion of particles in a sheared 2D LJ glass. $P(\Delta y, \Delta n)$ is the distribution of transverse motion Δy between Δn shear steps in AQS simulations. It corresponds to the Van Hove analysis for local dynamics in glassy systems. $\Delta y.P(\Delta y, \Delta n)$ or $P(ln\Delta y, \Delta n)$ shows clearly a cross-over from a non-Gaussian to a Gaussian distribution with a single maximum whose position evolves like $\Delta n^{1/2}$ (corresponding to diffusive motion). The contribution of the plastic displacements is enhanced in the last figure on the right, which shows that the Gaussian distribution is due to plastic displacements. Reproduced with permission from Springer Science + Business Media: Tanguy A *et al* 2006 *Eur. Phys. J.* E **20** 355.

the effective viscosity η follows Herschel–Bulkley law with approximately the same strain-rate dependence $\eta \equiv (\sigma_{\text{flow}} - \sigma_{\text{AQS}})/\dot{\gamma} \propto \dot{\gamma}^{-m'}$, with $m' = 0.5 \sim 0.6$ as deduced from figure 6(*b*). This is in agreement with a Maxwell-like interpretation of the viscosity where $\tau_\alpha = \eta/\mu$, μ being the shear modulus [47]. Tsamados [261] proposed an interpretation of this dependence of the relaxation time with $\dot{\gamma}$. The idea is that the rheological behavior of the amorphous material results from the competition between the propagation and nucleation of plastic rearrangements. The typical distance between thermally activated nucleated sites in a 2D system is $d_{\text{n}} = 1/(\rho_{\text{n}}\dot{\gamma}t)^{1/2}$ where ρ_{n} is a density of nucleated sites per unit strain, depending probably on T. The typical distance covered by mechanically-triggered plastic rearrangements due to the diffusion of plastic activity [165, 228, 256] from a given site is $d_{\text{p}} = (D_{\text{p}}t)^{1/2}$. If we assimilate the relaxation time to the time at which $d_{\text{n}} = d_{\text{p}}$, we obtain:

$$\tau_\alpha = \frac{1}{\sqrt{\rho_{\text{n}}\dot{\gamma}\, D_{\text{p}}}} \propto \dot{\gamma}^{-0.5}, \tag{9}$$

in agreement with the previous discussion.

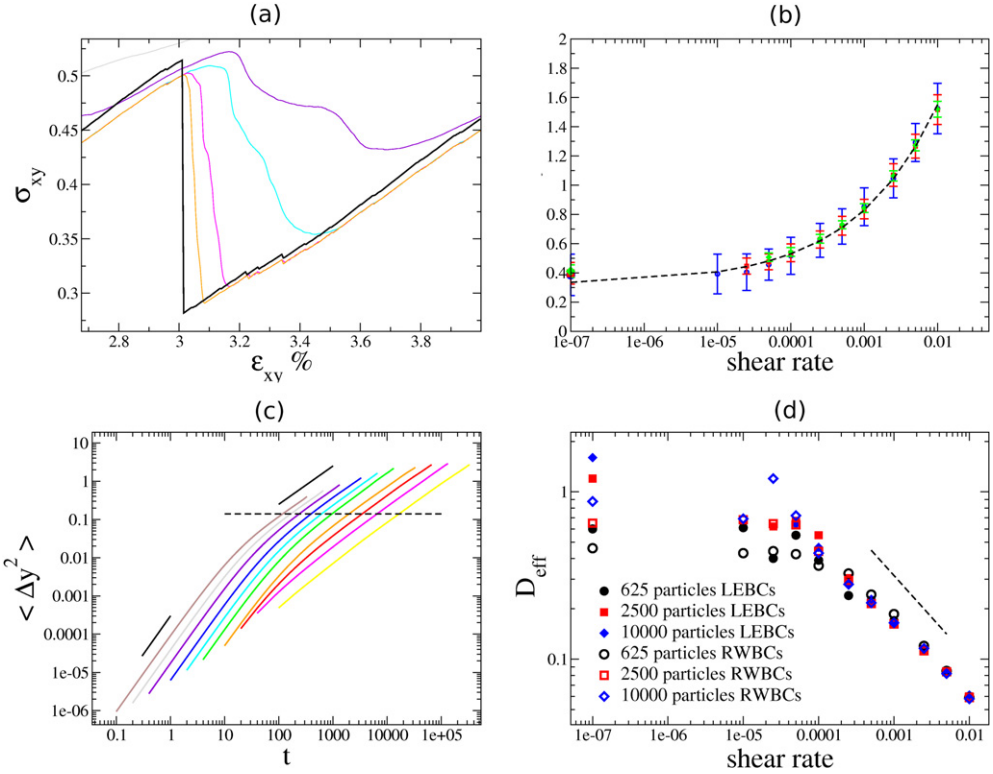

Figure 6. (*a*) Stress–strain relation during the MD simulation of a sheared 2D LJ glass with Lees-Edwards boundary conditions, for different shear rates $\dot{\gamma} = 1 \times 10^{-5}$, 2.5×10^{-5}, 5×10^{-5}, 1×10^{-4} and a AQS protocol (black line). (*b*) Rheological law $\sigma_{\text{flow}}(\dot{\gamma})$. The dotted line is an Herschel–Bulkley law $\sigma_{\text{flow}} = \sigma_{\text{QS}} + A\dot{\gamma}^{0.4}$. (*c*) Transverse mean-square displacement $\langle \Delta y^2 \rangle$ of the particles as a function of time for different shear rates. (*d*) Effective diffusive coefficient $D_{\text{eff}} = \langle \Delta y^2 \rangle / 2\Delta\gamma$. The dashed line corresponds to a power law $D_{\text{eff}} \propto \dot{\gamma}^{-0.5}$. Reproduced with permission from Springer Science + Business Media: Tsamados M 2010 *Eur. Phys. J.* E **32** 165.

In the well-defined athermal regime, the rheological law of the system is thus a Herschel–Bulkley law (equation (8)) and the dynamics is entirely due to the succession of plastic rearrangements that enable to recover a diffusive memory-free behavior for the particles, with possible $\dot{\gamma}$-dependence. Note, however, that finite-size effects are very important at small $\dot{\gamma}$, especially in the AQS regime, and they disappear only for sufficiently large strain rates, typically $\dot{\gamma} > 10^{-4}$ (see figure 6(*d*)). The diffusion coefficient then becomes a well-defined intensive (i.e. size independent) parameter, with a finite non-zero value even at very small temperatures.

In another study of the mechanical behavior of glassy materials at low temperature, Varnik and Raabe [274] proposed to consider the case where the heat created by plastic deformation is dissipated very efficiently by the system. This situation appears when the time needed to dissipate heat $t_{\text{d}} = L/c$, with c the sound wave velocity, is much smaller than the time needed to generate an energy $Nk_{\text{B}}T$ by plastic activity. The rate of heat production by plastic activity being $V\sigma_{\text{flow}}\dot{\gamma}$, the time needed to generate the energy $Nk_{\text{B}}T$ is $t_Q = Nk_{\text{B}}T/V\sigma_{\text{flow}}\dot{\gamma}$ and the condition $t_{\text{d}} \ll t_Q$ yields

$$\dot{\gamma} \ll \frac{\rho k_{\text{B}} T c}{L\sigma_{\text{flow}}}. \tag{10}$$

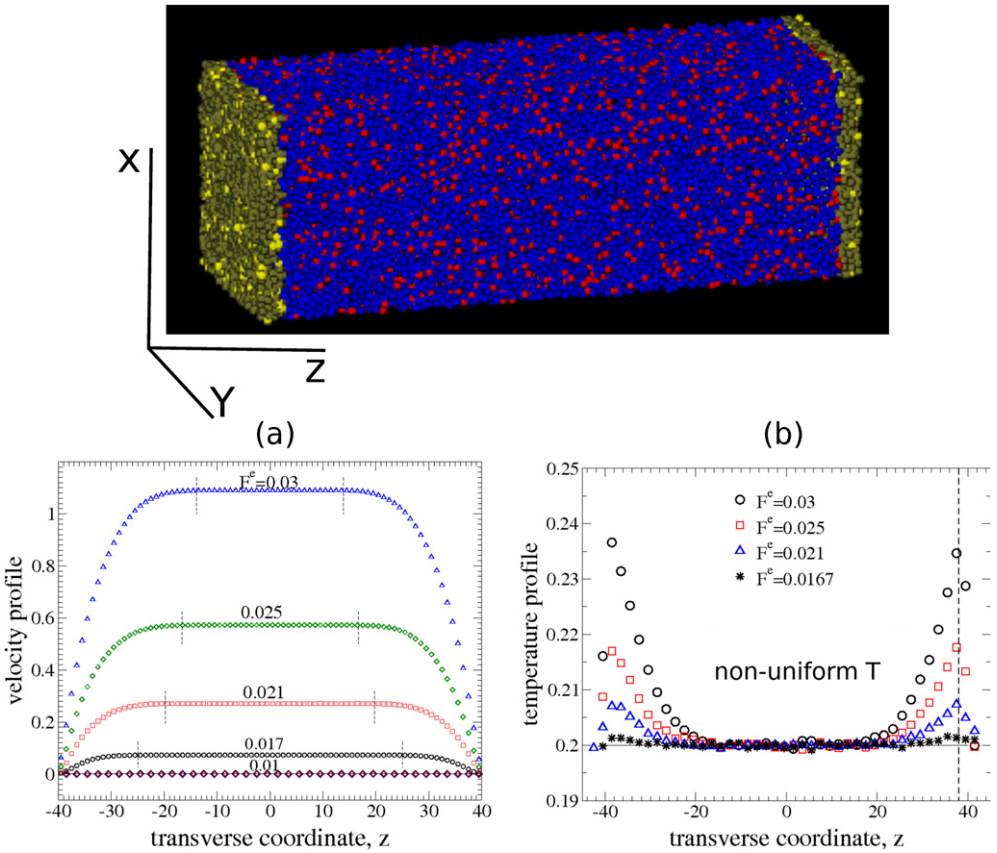

Figure 7. Shear velocity $v_x(z)$ and non-uniform temperature profile $T(z)$ in a Poiseuille-like flow of 3D binary LJ glass. Reproduced with permission from Varnik F and Raabe D 2008 *Phys. Rev.* E **77** 011504. Copyright (2008) by the American Physical Society.

The above relation is very different from the athermal condition in equation (7) and may be considered opposite because now the temperature plays a crucial role: the fact that the thermal energy is evacuated very efficiently assumes the presence of high thermal agitation. In this situation, as illustrated in figure 7, maintaining a uniform temperature profile inside the system is difficult, especially where the local shear rate is important, for example close to the walls where the flow is liquid-like (even if the temperature is far smaller than the melting temperature). This effect may also depend on the choice of thermostat (velocity rescaling in the direction transverse to the principal flow only [274]). The result we would like to emphasize here is that the interaction between the local temperature and local shear rate can affect the local dynamics and that local temperature and local dynamics are strongly coupled in atomistic simulations as soon as we depart from the athermal regime.

Indeed, identifying a single characteristic temperature for the rheological behavior of driven amorphous solids is very difficult. By looking at the detailed statistics of stress jumps in the atomistic simulations of the stress–strain curve of a binary glass (with a Berendsen thermostat), Karmakar *et al* [124] proposed to identify two main characteristic temperatures and showed that thermal fluctuations and strain rate define separate cross-overs in the dissipative behavior of the system as a function of system size. The cross-over due to thermal fluctuations

is obtained by comparing the energy dissipated during plastic rearrangements $\langle \Delta U \rangle / N$ to the thermal energy $k_B T$. The finite-size scaling of $\langle \Delta U \rangle$ allows to define a characteristic length ξ_2 at which both energies coincide. For $T = T_{\text{cross}}(L)$, $\xi_2 = L$, and if $T > T_{\text{cross}}$ $\xi_2 < L$. If $T < T_{\text{cross}}$, thermal agitation does not affect the stress drops and the corresponding plastic rearrangements have large size dependence, while if $T > T_{\text{cross}}$, plastic rearrangements are localized with a finite extent. We should note that this assumption relates the size of a plastic event (function of ΔU) to its energy barrier (only barriers of order $k_B T$ are accessible), but such relation may not be true in all systems [203]. The other cross-over is due to high strain rates. It allows to define another characteristic length ξ_1 by comparing, in a way analogous to the work of Varnik *et al* [274] discussed in the previous paragraph (except that here the temperature plays no role because it is replaced by the structural energy losses), the time needed to dissipate energy through sound propagation t_d, to the time needed to create plastic energy $t_P = \langle \Delta U \rangle / (V.\sigma_{\text{flow}} \dot{\gamma})$. The condition $t_d \ll t_P$ corresponds to $L < \xi_1$ that is to an AQS process with shear-rate independent sizes of plastic rearrangements but strong system-size dependence. Karmakar *et al* [124] proposed to recover the Herschel–Bulkley law for the flow stress by looking at the $\dot{\gamma}$-dependence of ξ_1 that dominates the plastic processes at large $\dot{\gamma}$ (when $\xi_1 < L$ or equivalently $t_d > t_P$). Finally, the comparison between the thermal effects and the shear-rate dependence can be done by comparing ξ_1 and ξ_2. For $\xi_1 < \xi_2$ the shear-rate dominates the plastic processes. It corresponds to small temperatures $T < T^*$ or equivalently to large values of $\dot{\gamma}$. For $\xi_2 > \xi_1$ ($T > T^*$), the temperature dominates the plastic processes. This description is supported by numerical results on a specific system [124]. However, the different exponents obtained depend on the system-size dependence of the stress-rearrangements during plastic events. Also, it has been shown recently that the extent of plastic rearrangements strongly depends on the details of the interatomic potential used, and in particular on three-body terms [86]. The above analysis has been deduced from a very specific system. It thus does not reflect the surprising universality of rheological laws of disordered systems, but a more appropriate dynamical analysis is still lacking at the moment. It can, however, be concluded that MD simulations support the idea that the relative values of T and $\dot{\gamma}$ must be considered very carefully.

Thermally activated transitions in MF descriptions of the energy landscape. Another way to take temperature into account, far above the athermal regime, is to consider the global thermal escape in a MF description of the saddle-node bifurcation preceding a plastic rearrangement [40]. When approaching a plastic instability, the global energy barrier presents the universal scaling form $\Delta E \propto (\gamma_c - \gamma)^{3/2}$ corresponding to a saddle-node bifurcation at γ_c [40, 124, 161], as discussed in section 3.1. Considering the energy barrier as a function of γ only, and not the other possible directions of the configuration space (this is why the model is of MF type), i.e. along the strain direction introduced in section 3.1 and assuming that the system is at equilibrium along all other directions, the Kramers expression for the activation rate is

$$R(\gamma) = \omega \exp\left(-\frac{\Delta E}{k_B T}\right). \tag{11}$$

Assuming a constant strain rate $\dot{\gamma}$, the probability $P(\gamma; \gamma_0)$ that the system has not yet flipped at strain γ starting from an initial strain γ_0 (survival probability [268]) is

$$\begin{aligned} P(\gamma; \gamma_0) &= \exp\left(-\frac{1}{\dot{\gamma}} \int_{\gamma_0}^{\gamma} \mathrm{d}\gamma' R(\gamma')\right) \\ &= \exp\left(-\frac{2}{3}\frac{\nu}{\dot{\gamma}}\left(\frac{T}{B}\right)^{5/6} (Q(\delta\gamma) - Q(\delta\gamma_0))\right), \end{aligned} \tag{12}$$

where $\delta\gamma = \gamma_c - \gamma$ and $Q(\delta\gamma) = \Gamma(5/6;\, B\delta\gamma^{3/2}/T)$ where Γ is the upper incomplete gamma function. P presents a very sharp transition from $P \approx 1$ to $P \approx 0$ around a strain γ^* such that

$$\frac{2}{3}\frac{\nu}{\dot{\gamma}}\left(\frac{T}{B}\right)^{5/6} Q(\delta\gamma^*) = 1. \tag{13}$$

Considering that the flip event due to the thermal activity occurs at that threshold, the macroscopic stress should thus be of the form

$$\sigma(\dot{\gamma}, T) = \sigma_0(\dot{\gamma}) - \mu\langle\delta\gamma^*(\dot{\gamma}, T)\rangle \tag{14}$$

where $\sigma_0(\dot{\gamma})$ is the athermal limit, μ is the shear modulus and $\langle . \rangle$ the average over structural disorder. As seen above (equation (8)), $\sigma_0(\dot{\gamma})$ follows a Herschel–Bulkley law $\sigma_0(\dot{\gamma}) = A_0 + A_1\dot{\gamma}^m$. The last term in the rhs of equation (14) provides the departure from Herschel–Bulkley law due to thermal activation in a MF approximation. It reads, after solving equation (13), to leading order in $T/B\delta\gamma^{3/2}$. :

$$\sigma(\dot{\gamma}, T) = A_0 + A_1(\dot{\gamma})^m - A_2T^{2/3}\left(\ln\left(A_3T^{5/6}/\dot{\gamma}\right)\right)^{2/3}. \tag{15}$$

This relation between T and $\dot{\gamma}$ is highly non-trivial and shows clearly that T and $\dot{\gamma}$ do not play similar roles that could be described through a simple scaling. Figures 8(a) and (b) show fits of the flow stress for a sheared binary LJ glass using the above relation at different strain rates and temperatures, with a single set of parameters, A_0 through A_3 [40], showing the high accuracy of equation (15). It must be noted that the same kind of law also describes very well the rheological properties of metallic glasses [121], as shown in figure 8(c).

The above expression does not explain the Herschel–Bulkley law obtained at very low temperature. Understanding the origin of this law probably requires a detailed description of the competition between local thermal escapes and elastically assisted propagation of plastic rearrangements, far from a simple-MF description, as mentioned in [261]. Such detailed description is still lacking, but efforts in this direction are made by a detailed analysis of the evolution of energy barriers with the temperature and strain rate. It has been shown, for example, [203] that while the statistics of activation energies changes drastically upon an applied stress, only the low range of the distribution is visited during thermal dynamics. The study of the detailed evolution of the density of selected energies with temperature and strain rate, as well as the precise way of escape (localized or collective rearrangements) should contribute to a better understanding of the respective roles of temperature and strain rates. It has also been shown [257] that even at zero temperature, the proximity to a plastic rearrangement (quadrupolar rearrangement or elementary shear band) affects not only the low-energy distribution of activation energies, but also the low frequency eigenmodes of the system, and thus the detailed accessible rearrangements. The respective occurrence of thermal escapes and mechanical vanishing of activation barriers can thus give rise to a variety of different behaviors.

Effective temperature. A general way to take into account the different roles of thermal and mechanical activity is to introduce an *effective temperature*. This tentative reconciling view is possible when the average behavior of the system can be described in terms of the linear response theory, with a linear relation between the response function to a perturbation and the corresponding correlation function—as in the usual fluctuation–dissipation theorem [50] (we note that another definition of the effective temperature has been proposed, based on the thermodynamics of the slowly evolving glass structure, i.e. the entropy and temperature of the structural degrees of freedom [29, 79]). In the domain of linear response, MD simulations showed that the fluctuations in the steady-state flow regime of sheared binary LJ glasses

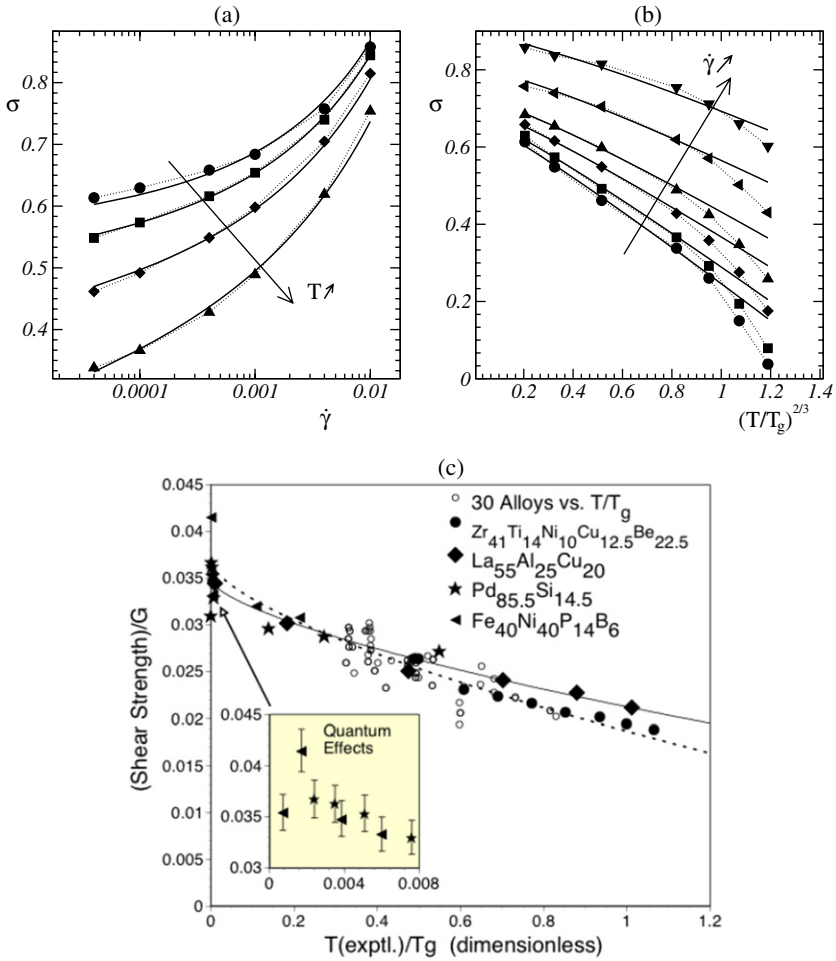

Figure 8. Temperature-dependent rheology: (*a*)–(*b*) Flow stress σ as a function of shear rate $\dot{\gamma}$ and temperature T in a 2D binary LJ glass. The continuous lines correspond to the parameterized rheological law in equation (15). Reproduced with permission from Chattoraj J *et al* 2010 *Phys. Rev. Lett.* **105** 266001. Copyright (2010) by the American Physical Society. (*c*) Experimental measurements of the flow stress as a function of $\dot{\gamma}$ for different metallic glasses close to T_g. The dashed line is a fit analogous to equation (15). Reproduced with permission from Johnson W L and Samwer K 2005 *Phys. Rev. Lett.* **95** 195501. Copyright (2005) by the American Physical Society.

[22, 23] and model foams [184] are comparable to those in equilibrium systems maintained at an *effective temperature* higher than the true temperature and function of the shear rate. More precisely, when the true temperature is above T_C (supercooled regime), the effective temperature converges to the true temperature T as the strain rate goes to zero, while for true temperatures below T_C (glassy regime), the effective temperature remains above T_C, with a limiting value different from T and close to T_C when the strain rate goes to zero [99]. In addition to steady-state fluctuations, the rate of activated transitions above energy barriers [111] and the steady-state stresses [99] are also functions of the effective temperature T_{eff} with Arrhenius dependence of the form $\exp(-\Delta E/k_B T_{\text{eff}})$. However, strong deviations from the linear behavior may appear, especially when the fluctuations become slow variables [213]. Moreover, as evidenced by equation (15), temperature and strain rate do not play equivalent roles in

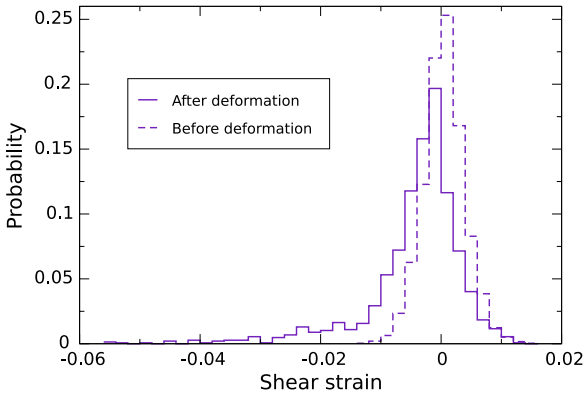

Figure 9. Distribution of strain of thermally activated events in the configuration quenched at 2×10^{-5} in figure 9, before deformation (dashed line) and after deformation and unloading to a shear-stress free state (solid line). The transitions are the same as in figures 3(*d*) and (*e*).

thermally activated transitions. Also, computer simulations showed that the succession of ISs visited under deformation is distinct from the ISs visited by equilibrated systems [113, 138]. In particular, the average IS energy in a sheared system at a given effective temperature is higher than the average IS energy of the same system maintained in equilibrium at a temperature equal to the effective temperature [99]. Finally, The range of validity of the effective temperature description thus still needs to be delimited clearly in out-of-equilibrium systems.

Polarization. Another reason why heating and mechanical deformation cannot be strictly equivalent is that plastic deformation can induce anisotropy in the glass microstructure whereas heating cannot. Structural anisotropy is referred to as *polarization* [12] and is the hallmark of history-dependence in glasses. It is at the origin of several of the mechanical characteristics of glasses, such as the Baushinger effect [78] and anelasticity, i.e. time- and temperature-dependent recovery of glasses after deformation [9, 12]. Polarization has been measured experimentally in metallic glasses through x-ray diffraction spectra that become anisotropic after plastic flow in uniaxial tension [248] and compression [186]. The results indicate that during deformation bonds are reorganized such that in tension, bonds in the tensile direction are cut and reform in the transverse direction, and vice versa in compression. Bond anisotropy has been reported in MD simulations of a silica glass [208] by considering the fabric tensor $\boldsymbol{F} = \langle \boldsymbol{n} \otimes \boldsymbol{n} \rangle$, where $\boldsymbol{n}$ is the unitary bond vector between atoms, and associated anisotropic parameter $\alpha = \sqrt{3/2 \sum_{i=1}^{3} (\lambda_i - 1/3)^2}$, where $\{\lambda_i\}$ are the eigenvalues of $\boldsymbol{F}$. Polarization is more difficult to evidence in simulated metallic glasses, presumably because the lack on angular dependence of the interatomic potentials used to model metallic glasses (see section 2.1) imposes fewer constraints on bond angles. The anisotropic parameter does not vary with plastic strain in metallic glasses [204], but bond anisotropy was reported by computing an anisotropic pair distribution function under zero stress [74, 260]. In the extreme case of monodisperse amorphous systems with two-body interactions and no directional bonding, crystallization can even occur [177] at a sufficiently large strain whose critical value increases with strain rate. Polarization in metallic glasses is also visible through their local PEL, by considering the distribution of strains associated with thermally activated transitions around deformed configurations [203, 204]. Examples of distributions are shown in figure 9 for the most slowly quenched glass of figure 3. Before deformation, the distribution of strain is symmetrical

around zero, while after deformation and relaxation to zero stress, the strain distribution is asymmetrical and contains more events with a negative strain, i.e. opposite to the initial direction of deformation, than events with a positive strain, i.e. in the same direction as the initial deformation. This asymmetry explains anelasticity since relaxation from a deformed state will tend to remove the anisotropy and will involve more events with a negative strain than a positive one, thus producing an average deformation in the direction opposite to the initial direction of deformation, as was checked by activated dynamics in a 2D LJ glass [204].

4. Mesoscopic models

From the atomistic simulations reviewed above, we know that plasticity in glasses occurs by local plastic rearrangements, or STs, that have a characteristic size ℓ_{ST} on the order of a few nanometers. The cost for the high level of details in atomistic simulations is a strong limitation in both length- and time scales (typically a few tens of nanometers during a few tens of nanoseconds as seen in the previous section). In order to access larger scales while retaining a description of the elementary dissipative plastic processes, we wish now to develop a model for amorphous plasticity at the mesoscopic scale that averages out atomistic effects and accounts only for the dynamics of STs, in the same way as dislocation dynamics describes crystal plasticity based on the motion, multiplication and interaction of dislocations without explicitly accounting for atomic-scale core effects [156].

Generally speaking, a mesoscopic model requires four elementary ingredients: (i) a *local yield criterion* for the occurrence of plastic rearrangements, (ii) an *elastic coupling* to represent the reaction of the elastic matrix to the local rearrangements of the amorphous structure, (iii) an *evolution rule* for the local yield criterion because a plastic rearrangement alters locally the amorphous structure, leading to either local softening or hardening of the matrix, (iv) a *dynamical rule* to associate a time scale to the elementary processes. In analogy with atomistic simulations, depending on whether the temperature range considered is far below or close to the glass transition, the simulations can be conducted in the AQs limit or time and temperature may be accounted for using for example a kinetic Monte Carlo algorithm. The above elementary ingredients are reviewed below.

As an introductory illustration, directly inspired by the work of Dahmen *et al* [52, 83] and more generally by depinning models of driven interfaces in random media [123, 151], we present below a general equation of motion that incorporates the elementary building blocks mentioned above:

$$\eta \frac{\partial \varepsilon(\boldsymbol{x}, t)}{\partial t} = \mathcal{H}\left\{\sigma_{\mathrm{ext}} + \sigma_{\mathrm{int}}(\boldsymbol{x}, t) - \sigma_{\gamma}\left[\varepsilon, \boldsymbol{x}, \{\varepsilon(\boldsymbol{x}, t' < t)\}\right]\right\}, \tag{16}$$

where

$$\sigma_{\mathrm{int}}(\boldsymbol{x}, t) = \int_0^t \mathrm{d}t' \int \mathrm{d}\boldsymbol{x}' J(\boldsymbol{x} - \boldsymbol{x}', t - t')[\varepsilon(\boldsymbol{x}', t') - \varepsilon(\boldsymbol{x}, t)]. \tag{17}$$

We are here restricted to a scalar formulation where ε is the local shear strain, σ_{ext} is an applied shear stress, σ_{int} is the local shear stress accumulated at point $\boldsymbol{x}$ and time t due to elastic stress transfer from all previous STs since time $t = 0$ (where a fully relaxed—unstressed—configuration is assumed) and σ_{γ} is a random pinning stress (local yield stress) that prevents plastic slip until the local stress ($\sigma = \sigma_{\mathrm{ext}} + \sigma_{\mathrm{int}}$) exceeds the local threshold. η is an effective viscosity that sets the characteristic relaxation rate and $\mathcal{H}$ is the Heaviside step function. This generic example shows how one may build an equation of motion from a small number of hypothesis in terms of a mesoscopic description of threshold criteria, elastic coupling and dynamics, that can then be solved numerically—or sometimes analytically.

4.1. Elementary ingredients of a mesoscopic model

Local yield criterion. A mesoscopic model involves a discretization length, ξ, and the first question to be asked is how to choose ξ with respect to ℓ_{ST}. This choice does not appear clearly in the definition of most models proposed in the literature and ξ may actually be either close to or significantly larger than ℓ_{ST}, depending on the model considered. Related to the choice of ξ is the question of using whether a local or non-local yield criterion for the plastic reorganizations and on what internal variable should the criterion be based. Indeed, at the continuous scale, all plastic criteria so far have relied on the local stress state of the material. The well-known Tresca and von Mises criteria for instance impose a limit, or yield surface, to well-chosen norms of the deviatoric part of the local-stress tensor (maximum deviatoric stress for Tresca, and maximum deviatoric elastic energy for von Mises). More elaborated criteria can be defined to take into account the pressure dependence [128, 205, 230]. On the other hand, at the atomistic scale, we have seen in section 3.1 that a stress-based criterion for ST nucleation is not the most relevant because plastic reorganizations are better predicted by a lowering of the local elastic shear modulus.

Relating non-local effects and elastic moduli-based criteria at the atomic scale to the well-established relevance of local stresses at the continuous scale is a very challenging task that has so far received little attention in the literature, probably due to its inherent difficulty. One way to circumvent (or reformulate) this question is to identify the relevant spatial scale ξ at which mesoscopic modeling may be performed. Indeed, one may expect that non-local contributions that are significant at the reorganization length scale ℓ_{ST} are averaged out in a description at a slightly larger length scale (say $10\ell_{\mathrm{ST}} \approx 3$ nm in a mineral glass), while preserving the information on the dissipative reorganization due to the STs.

In practice, mesoscopic models assume homogeneous linear elasticity, such that the discrete scale ξ should be significantly larger than the microscopic length scale ℓ_{ST}. Then, mostly for the sake of simplicity, most models assume a simple (scalar) stress-based criterion:

$$\sigma(\boldsymbol{x}) = \sigma_{\mathrm{Y}}(\boldsymbol{x}) \tag{18}$$

where σ is the local shear stress (or shear stress invariant of the stress tensor) and σ_{Y} is the *local yield stress* at location $\boldsymbol{x}$, also called slip or failure stress, i.e. a ST is triggered at $\boldsymbol{x}$ if $\sigma(\boldsymbol{x}) > \sigma_{\mathrm{Y}}(\boldsymbol{x})$. The local yield stress can be chosen spatially homogeneous [196, 197] or heterogeneous [18, 52, 116, 250], with consequences discussed below.

An alternative way that includes thermal activation is based on an energy approach at the ST scale [32–34, 106, 107]. While keeping the hypothesis of elastic homogeneity, the authors used a lattice defined at a sub-ST scale ($\xi < \ell_{\mathrm{ST}}$) and estimated the energetic cost of local plastic shears involving sets of neighboring cells to recover a length scale $\sim \ell_{\mathrm{ST}}$. The energy cost is computed as

$$\Delta E = \Delta F_0 - \sigma(\boldsymbol{x})\frac{\gamma_{\mathrm{p}}\Omega_0}{2}, \tag{19}$$

where ΔF_0 is the stress-free activation free energy of a ST, biased by the work of the local stress between the initial and activated configurations, $-\sigma\Omega^*$, where σ is the local stress resolved on the plane and direction of shear of the ST and $\Omega^* = \gamma_{\mathrm{p}}\Omega_0/2$ the activation volume with γ_{p} the strain associated with the ST and Ω_0 the volume of the ST. In [107], the plastic strain increment γ_{p} was chosen constant, equal to 0.1 in agreement with the Lindemann criterion observed at the atomic scale (see section 3.1). The volume of the ST Ω_0 was also constant, taken equal to 1.6 nm^3 to reproduce the properties of Vitreloy 1, a commercial metallic glass, i.e. contains 84 atoms, again in agreement with the atomistic simulations presented in section 3.1. We should note that within this approach, if an athermal yield criterion is applied, stating that plastic

events occur when their activation energy vanishes, a local homogeneous stress-based yield criterion is recovered, as in equation (18), with a yield stress $\sigma_Y = \Delta F_0/\Omega^*$.

Evolution rule for the yield criterion. Another crucial point concerns the evolution of the possible values of the yield criterion under plastic deformation. Indeed, after a reorganization has occurred, the local structure of the glass is altered, which may change its local yield stress. In some models proposed in the literature, the local yield stress in equation (18) is unchanged after plastic slip [32, 106, 107, 196, 197] implying a homogeneous and stationary yield-stress landscape. In other models, the yield stress is renewed based on a specific rule: the new value may be drawn from a stationary distribution without correlation [18, 250] or may be systematically increased (respectively decreased) [52], which naturally leads to hardening (respectively softening). We should note that using a stationary distribution also leads to hardening during the initial stage of deformation by a progressive exhaustion of the weakest sites in the configuration [250]. Two different distributions (one for the initial configuration and the other for renewing the yield stresses under deformation) have also been used to model aging [270] (see below).

Elastic coupling. Successive STs are not independent because the elastic medium surrounding the reorganizing zone reacts to the local change of conformation and acquires an additional (positive or negative) internal stress increment. The strength of this increment depends on the plastic strain associated with the ST, the size of the ST and the shear modulus [249]. While ST size and shear modulus have been so far systematically chosen constant, the plastic strain has been chosen either constant [32, 107] or drawn from a statistical distribution [18, 250].

Restricting ourselves to continuum mechanics, finding the elastic relaxation around a plastic ST is similar to the plastic inclusion problem treated early-on by Eshelby [76]. We will assume here as in previous paragraphs that the mesoscopic length scale is sufficiently large to allow for a continuum and homogeneous description of elasticity. Within this approximation, there are several ways to include elastic effects in mesoscopic models:

- *Mean field.* Ignoring the details of the elastic interaction, a first approach consists in assuming that the elastic relaxation of a reorganized region is compensated by a constant elastic stress everywhere else [52]. A statistical variant consists in drawing local elastic responses from an uncorrelated random distribution (constrained by the global balance of elastic contributions). Several distributions have been tested [145], from a simple Gaussian distribution to *ad hoc* distributions that mimic the effect of a quadrupolar Eshelby contribution (see below). An advantage of this approach is the possibility for analytical treatment [145, 272]. However, such an approach cannot capture the build-up of spatial correlations that will be shown to be an essential manifestation of the collective interplay between STs.
- *Exact numerical solution.* A second approach consists in solving numerically the equation of elastic equilibrium, thus accounting for the precise plastic strain induced by the ST and the outer boundary conditions. Elasticity can be solved using the FEM in direct space [107] or, if the lattice is regular, using Green's function, obtained as the elastic response of an elementary cell of the lattice to a unit shear [18, 32], or else using Lagrange multipliers [116].
- *Eshelby quadrupolar interaction.* An intermediate way consists in focusing on the dominant term of the elastic response at long distance. The Eshelby solution of the elastic field induced by a plastic inclusion can be developed using a multipolar expansion [249].

While at short distance several terms are necessary to account for the details of the plastic reorganizations, at long distance, only the dominant term of the expansion, proportional to $1/r^d$ (where d is the space dimension), survives. In two dimensions, such an analysis can be carried out using the complex potentials of Kolossov and Muskhelishvili [180]. It appears that only two terms survive at long distance. One is associated with the temporary dilation/contraction of a circular inclusion while the other term is associated with the local shear of a circular inclusion. This second term is responsible for the well-known quadrupolar symmetry of the elastic shear stress response:

$$\sigma_{xy} = -\frac{2\mu}{\kappa + 1}\frac{\mathcal{A}\gamma_{\mathrm{p}}}{\pi r^2}\cos(4\theta) \tag{20}$$

where μ is the elastic shear modulus and $\kappa = (3 - 4\nu)$ for plane strain and $\kappa = (3 - \nu)/(1 + \nu)$ for plane stress, ν being Poisson's ratio. This symmetry is visible for example, in the atomistic snapshot shown in figure 1(a). Note that in equation (20), the size of the zone under reorganization $\mathcal{A}$ does not contribute independently but through its product with the plastic strain, which is about twice the activation surface or activation volume in equation (19). γ_{p} being on the order of 0.1, the activation volume or surface is about a tenth of its actual size, in contrast with dislocations where γ_{p} is close to 1 and activation and real surfaces and volumes are identical. While *a priori* simple, the implementation of such quadrupolar solution on a discrete lattice happens to be numerically delicate. Satisfaction of the boundary conditions is made difficult by the long-range decay of the elastic interaction. To circumvent potential resummation problems in direct space, it is valuable to rewrite the interaction in Fourier space in case of periodic boundary conditions [197, 250].

Dynamical rule. As mentioned above, there are two main choices of dynamical rule for mesoscopic models, based on either a quasistatic or a kinetic Monte Carlo algorithm. In the *quasistatic limit*, thermal and rate effects are ignored and the dynamics is entirely dictated by the satisfaction of the local yield criterion. The system can be either stress- or strain-driven using two simple numerical protocols inherited from the field of self-consistent criticality [188, 233]. The first protocol, called *extremal dynamics* [18, 250] consists in allowing one and only one event per simulation step, i.e. the weakest site in the configuration. The applied stress (called extremal stress) is thus adapted at each step to induce only this event and therefore results in a vanishing shear rate. In the algorithm, the weakest site is first identified and subjected to a local plastic strain, the associated local yield stress is renewed (or not) according to the chosen rule of evolution and the stress field is updated to account for the internal stress change induced by the local transformation. Finally the whole process is iterated. While the shear strain rate is reduced to its lowest possible numerical value, the associated extremal stress strongly fluctuates. The macroscopic yield stress is then identified as the maximum extremal stress.

The second quasistatic protocol consists of *slowly (quasistatically) increasing the applied stress* [52, 197]. For a given value of the external stress, all sites satisfying their local yield criterion experience a shear strain increment. As before, the yield criterion and internal stress are then updated, but in contrast with the previous driving mode, the applied stress is unchanged. Thus, the new configuration may contain a new set of sites that satisfy the yield criterion, i.e. the occurrence of some local slip may trigger other local slip events, leading to *avalanches*, as seen in the atomistic simulations in section 3.1. The procedure is then iterated at constant applied stress until the avalanche eventually stops, when a configuration is reached where no site satisfies the yield criterion. Only then is the external stress increased by a small amount and

the whole procedure is started again. In this approach, the number of sites experiencing slip increases with external stress and diverges when the macroscopic yield stress is reached [197].

Note that the bulk elasticity of the material and/or the compliance of the mechanical testing machine can be incorporated by coupling the system to a spring [255, 285]. Tuning the value of the spring constant then allows to drive the system, imposing either a strain (high spring constant) or a stress (low spring constant).

The above protocols suffer from a clear drawback: any notion of realistic time has disappeared since the number of iterations simply counts the number of plastic rearrangements and avalanches in the system; or said in other words, while the iterations give successive configurations of the system, the time scale separating the configurations is unknown. One way to introduce a time scale and at the same time thermal effects is to employ a *kinetic Monte Carlo algorithm*. This approach has been used in conjunction with the energy-based criterion in equation (19), which provides the activation energy of potentially thermally activated STs [32, 106, 107]. From a given configuration, all potentially thermally activated events are first determined. The activation energy of each event is calculated, from which the distribution of rates of the events is obtained using Boltzmann statistics. One event is then drawn from the distribution. Stresses, activation energies and rates are then updated and the whole procedure is iterated. This approach was developed in two [32, 107] and three dimensions [108] and was shown to reproduce the mechanical properties of metallic glasses, including the high-temperature homogeneous flow and the low-temperature strain localization in shear bands.

Another approach to include a time scale and to account for rate effects (but not for thermal effects) within a simple yield-stress model consists in assigning characteristic transition times for a region to either plastically (viscously) deform or to relax back to an elastic state. The most striking rate effect is that shear bands occur in complex yield-stress fluids only at low strain rates while at higher strain rates, homogeneous flow is recovered [48, 49, 141, 187]. One of the first models of this family, developed to simulate the rheology of complex fluids, is due to Picard *et al* [197]. In this model, the displacement is discretized on a lattice and each site can be either in an active *plastic* (or more exactly visco-plastic) state if its local stress is larger than a yield stress or in a still *elastic* state in the opposite case. Characteristic transition rates τ_{pl}^{-1} and τ_{el}^{-1} are then assigned for the transition from elastic to plastic for an active site and from plastic to elastic for an inactive site. When a site becomes 'plastic', its strain relaxes through Maxwell dynamics, i.e. with a rate proportional to the local stress: $\dot{\gamma}_{\mathrm{p}} = \sigma/2\mu\tau$ where μ is the shear modulus and τ a mechanical relaxation time (in practice, the authors chose $\tau_{\mathrm{pl}} = \tau_{\mathrm{el}} \equiv \tau$ and have thus a single time scale). The plastic strain produces an internal stress by its associated Eshelby field. Although simple, this elasto-plastic model produces complex spatio-temporal patterns of deformation [167] and includes both Newtonian and non-Newtonian regimes with a threshold strain rate $\sigma_{\mathrm{Y}}/\mu\tau$. However, we should note that τ_{pl} and τ_{el} are characteristic time scales, not directly related to microscopic processes so far.

Three model archetypes naturally emerge from the possible choices allowed by the different rules described above. All three models feature local plastic events that interact elastically. The first archetype, developed by Vandembroucq *et al* [18, 52, 250], which will be called the *depinning model*, is based on a yield-stress criterion with yield stresses and plastic strains drawn from statistical distributions, an internal stress arising from the accumulation of Eshelby fields and extremal dynamics. The second model, developed initially by Bulatov and Argon [32] and extended by Homer *et al* [106–108], called here the *KMC model*, is based on a kinetic Monte Carlo algorithm with an energy-based yield criterion and elasticity solved by the FEM. Here, the yield criterion is not affected by deformation and the ST plastic strain

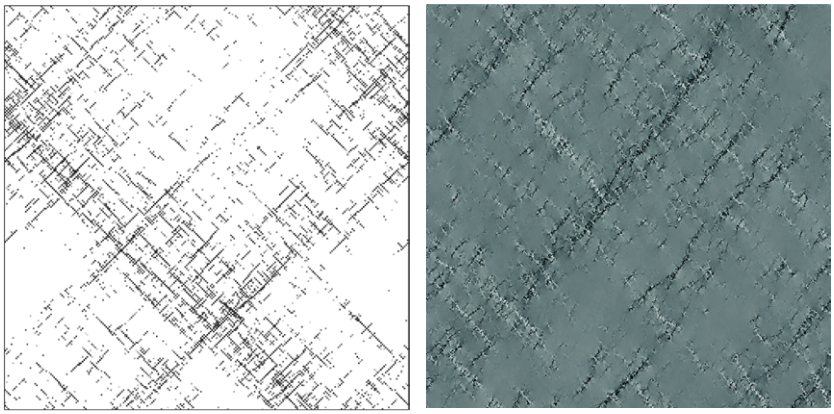

Figure 10. Comparison of activity maps between a mesoscopic model (left) and an atomistic simulation (right). Left: map of cumulated plastic activity in the stationary regime during a deformation window $\Delta\varepsilon = 0.01$ obtained with the mesoscopic depinning model. Reproduced with permission from Talamali M *et al* 2010 arXiv:1005.2463. Right: strikingly similar map of plastic activity (vorticity of the displacement field) computed on a 2D LJ binary glass under compression. Reproduced with permission from Maloney C E and Robbins M O 2009 *Phys. Rev. Lett.* **102** 225502. Copyright (2009) by the American Physical Society.

is constant. The third model, developed by Picard *et al* [26, 167, 196, 197], called a *fluidity model*, is based on a constant yield-stress criterion and Maxwellian viscous strain rate. It includes strain-rate effects through characteristic transition rates. In all cases, the dynamics of the systems is stochastic, reflecting the disorder inherent to glasses, but it is interesting to note that the origin of this disorder is modeled in different ways in the above models. The depinning model is based on what may be called a *structural disorder*, which arises from the stochastic distribution of local yield stresses (i.e. a structural internal variable), whereas the fluidity and KMC models have constant yield stresses (therefore no structural disorder) but reflect a *dynamical disorder*, which arises from the randomness of their dynamical rules, either through Boltzmann statistics for the KMC model, or through the stochastic distribution of the relaxation times for the fluidity model.

4.2. Phenomenology

We consider here three applications of mesoscopic models, namely a comparison with atomistic simulations, the interplay between aging and shear banding and avalanches in plastic flow.

Comparison with atomistic simulations. Figure 10 compares maps of plastic activities obtained with the depinning model [250] and with atomistic simulations (2D binary LJ glass [163]). The similarity between the two maps is striking. In both cases, plastic strain is spread over the entire system and one can clearly distinguish elongated patterns along the directions at $\pm\pi/4$. Those correlated events are transient localization events. They are observed with all models that satisfy elasticity equilibrium [32, 107, 116] and are due to the quadrupolar symmetry of the Eshelby field (equation (20)).

This comparison between atomistic and mesoscopic models clearly shows that the elementary ingredients included in the mesoscopic models, i.e. mainly localized plastic events that interact via the Eshelby stress field, are sufficient to reproduce the deformation pattern of some atomic-scale glasses and to some extent the anisotropic character of the plastic strain

power spectrum. We will see below other examples of processes where mesoscopic and atomistic simulations agree very well. We should note, however, that the comparison of post-mortem deformation patterns is a rather qualitative test. Comparing rheological properties such as $\sigma(\dot{\gamma})$ or the detailed spatio-temporal evolution of plastic damage could be more discriminating tests to guide the choice of the elementary ingredients to include in mesoscopic models.

Localization, shear banding and aging. Localization effects have been discussed early in the framework of mesoscopic models [18, 197]. More recent studies were devoted to shear banding [164, 165] and in particular its dependence on aging [82, 179]. Persistent shear bands form when correlations between plastic events are stronger than the disorder in the glass. Both disorder and correlations can be of structural and dynamical origins. Correlations are strongest in case of softening, i.e. *structural correlations*. There are also *dynamical correlations* because when a ST is triggered, the stress increment added to neighboring sites through the Eshelby field (equation (20)) may be larger than the local yield stress, leading to a succession of STs. The latter appear along elongated patterns because of the strong anisotropy of the Eshelby field. As mentioned above, there is *structural disorder* for instance when yield stresses are drawn from a random distribution [18] or when the configuration contains an initial elastic stress field [107, 116]. Disorder may also be dynamical when the glassy dynamics is itself stochastic, for instance when using a KMC algorithm. A *dynamical disorder* also arises from the slow decay of the Eshelby field at long range. Indeed, the Eshelby field of a ST affects distant regions in the glass. The succession of these stress increments plays a role analogous to a temperature (or effective temperature [234]) that can be regarded as an uncorrelated mechanical noise [145].

In summary, disorder and correlations can have structural and dynamical origins depending of the models and simulation conditions and the competition between these factors controls the formation of shear bands. In the absence of structural correlations (no softening), disorder is usually stronger than dynamical correlations and no persistent shear bands form. As illustrated in figure 10(*a*), the strain field is then characterized by an accumulation of transient localized patterns corresponding to successive small avalanches. In the absence of nucleation sources (walls or local structural defects) or local softening, such patterns diffuse throughout the systems and no persistent shear band forms. Only the anisotropic spatial correlation of the strain field retains a trace of the transient localization [18, 106, 163, 250].

In the absence of softening, persistent shear bands form when there is no structural disorder in the initial glass configuration or when structural disorder relaxes faster than the strain rate. The influence of initial conditions was demonstrated by Homer and Schuh [107] using the KMC model by preparing glasses that either contained an initial density of STs (activated during a quench from high temperature) and thus contained an initial structural disorder through an internal stress field, or contained no ST and were therefore stress-free without initial disorder. Only in the latter case, shown in figure 1(*b*), was a persistent shear band observed. Otherwise, the deformation pattern was similar to figure 10(*a*). Another example is if the initial configuration contains a distribution of stresses that relaxes during deformation, as in the work of Jagla [116]. Shear bands were observed only if the strain rate is small compared with the stress-relaxation rate, i.e. only if the configuration has time to relax to a stress-free configuration without structural disorder before plastic flow sets in.

Shear bands in complex fluids are thus limited to low strain rates because of a competition between the rate of production of structural disorder, which increases with strain rate $\dot{\gamma}$, and the rate of relaxation of structural disorder. Using a simple MF fluidity model, Coussot and Ovarlez [48] showed that the condition for shear band formation, using the notations introduced

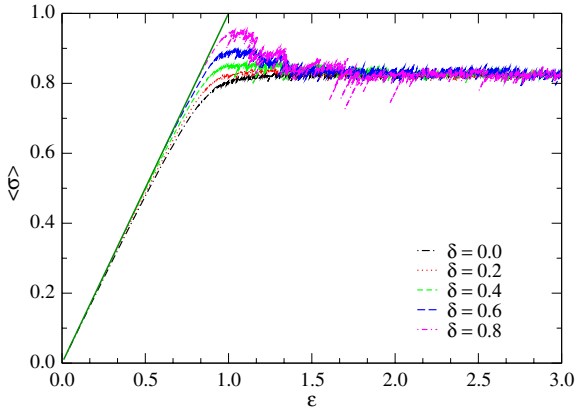

Figure 11. Effect of aging on the strain/stress curve in the depinning model. The aging parameter δ is the minimum normalized yield stress in the initial glass configuration before shearing. Reproduced with permission from Vandembroucq D and Roux S 2011 Shear banding behavior in glasses: a mesoscopic approach (unpublished).

here, is

$$\tau_{\mathrm{el}} > \tau \qquad \text{and} \qquad \dot{\gamma} < \sigma_{\mathrm{Y}}/\mu\tau_{\mathrm{el}}(\sqrt{\tau_{\mathrm{el}}/\tau} - 1). \tag{21}$$

In metallic glasses, it is also known that deformation is homogeneous at high strain rates [218] but the reason is different and is due to the fact that the strain per band is not sufficient to sustain the strain rate. Within the fluidity model, this situation may be related to the condition $\dot{\gamma} > \tau_{\mathrm{pl}}^{-1}$.

Shear bands are prominent in aged glasses where structural relaxations and local softening are accounted for. The effects of aging and stress relaxations have been studied using several mesoscopic models [82, 116, 179, 270]. Within the depinning model [270], aging was modeled by drawing the initial distribution of yield stresses from a statistical distribution shifted to higher stresses compared with the distribution used to renew the yield stress under deformation. More precisely, the initial yield stresses were drawn from a uniform distribution between $[\delta; 1 + \delta]$ in normalized units, while under deformation, the distribution was uniform between [0; 1]. The parameter δ, the minimum of the initial distribution, is called the *aging parameter* because the yield stress is expected to increase logarithmically with time during the aging process [179, 207]. The resulting stress/strain curves as a function of δ are shown in figure 11, where in agreement with atomistic simulations, as δ increases, i.e. as the glass ages, an upper yield point develops followed by a steady-state flow state independent of the initial configuration. Associated with the stress overshoot is the development of a shear band shown in figure 12. The reason is that after the first slip events, the new yield stress is drawn from a distribution with statistically lower yield stresses, which induces a systematic softening effect, thus leading to localization. In this approach, once the plastic activity has concentrated along a band, the system remains trapped for arbitrary long times while the band widens at a logarithmic pace. A similar correlation between initial stress overshoot and shear bands was obtained using fluidity models [82, 179] where the lifetime of the shear band appears bounded to the intrinsic time scale of the model.

A notable effect on shear banding can be obtained by tuning the level of the mechanical noise, which can be obtained by increasing the plastic strain increment per ST [270]. Starting from aged configurations, it appears that the higher the mechanical noise, the faster the shear band widens and the shorter its duration. Also, shear banding is strongly affected by the

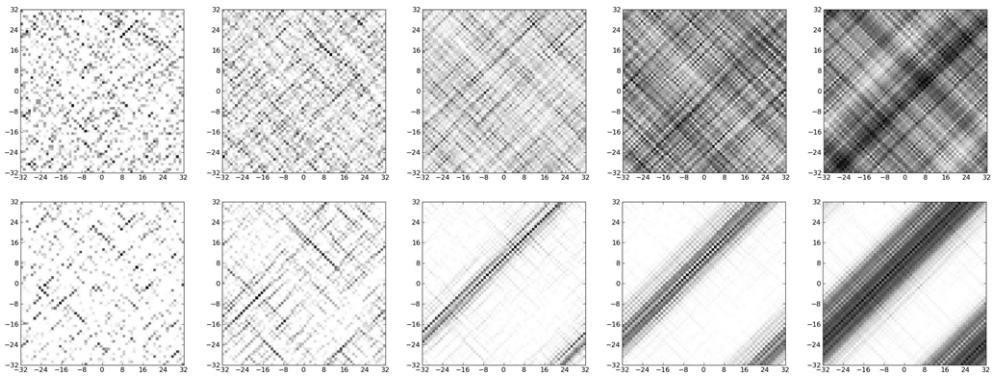

Figure 12. Maps of plastic strain obtained from left to right at strains 1/16, 1/4, 1, 4 and 16 and from top to bottom with an aging parameter $\delta = 0$ (top) and $\delta = 0.5$ (bottom). Reproduced with permission from Vandembroucq D and Roux S 2011 arXiv:1104.4863.

boundary conditions and is more readily obtained with fixed boundary conditions than periodic boundary conditions [197], as in atomistic simulations (see section 3.1).

Finally, we note that the way structural disorder is introduced in the above models is phenomenological and not related to any local structural defects, such as non-icosahedral environments or anomalous coordination numbers, as observed in atomistic simulations. It would thus be very interesting to relate the atomistic-scale structural parameters to appropriate mesoscopic variables, such as a relaxation time or a distribution of yield stresses.

Avalanches. Intermittent flow. While traditionally described in continuum mechanics by constitutive laws at the macroscopic scale, it has progressively appeared in the last two decades that the mechanical behavior of materials was not as smooth and regular as anticipated. In particular crack propagation in brittle materials and plastic flow in crystalline solids have been shown to exhibit jerky motion and scale-free spatio-temporal correlations [27, 174, 283].

In the context of plasticity of crystalline materials, a significant number of results have been obtained over the last decade (see, e.g., the comprehensive review by Zaiser about scale invariance in plastic flow [283]). Acoustic emission measurements performed on ice or metal monocrystals have shown a power-law distribution of the energy $P(E) \propto E^{-\kappa}$ with $\kappa \approx 1.6$ for ice [202] and $\kappa \approx 1.5$ for hcp metals and alloys [201]. The case of polycrystals is somewhat more complex since not only a grain size related cut-off appears in the avalanche distribution but the power-law exponent is also significantly lowered [202]. Performing nano-indentation measurements on nickel monocrystals, Dimiduk *et al* found evidence for a scale-free intermittent plastic flow and estimated $\kappa \approx 1.5$–1.6 [61]. Very recently analogous analysis was performed on metallic glass samples. Sun *et al* [247] measured the distributions of stress drops occurring in the stress/strain curves for various metallic glass samples under compression and observed scale-free distributions with a power law exponent $\kappa \in [1.37$–$1.49]$. MF models such as developed by Dahmen *et al* [51] give a power-law distribution for the size s of avalanches $P(s) \propto s^{-3/2}$ thus with an exponent strikingly close to the experimental results. Note that the introduction of systematic hardening [52] induces a finite cut-off in the initially scale-free distribution. Zaiser and Moretti [284] also measured a similar exponent in a dislocation-based model and found evidence for a stiffness-induced cut-off.

While from renormalization theoretical results, Dahmen *et al* [52] argue in favor of the universality of the MF exponent, a rapid tour of the other models reveals a more complex

situation. Starting from the closest member of the class, Lemaître and Caroli [145] obtained the MF result when using a statistical MF approach with a Gaussian distribution. Indeed the average size of avalanches was shown to scale as $\langle s \rangle \propto L^{0.5}$, consistent with a $s^{-3/2}$-distribution. However, when using an uncorrelated random noise reproducing the quadrupolar Eshelby field, they obtained a clearly different scaling with $\langle s \rangle \propto L^{0.14}$. This strong dependence on the distribution may not be as surprising as it may appear at first. Indeed, the latter Eshelby-like noise happens to exhibit fat power-law tails.

Using a full Eshelby elastic interaction, Talamali *et al* [251] obtained an avalanche scale-free distribution with an exponent $\kappa = 1.25$. While significantly different from the MF prediction, this non-trivial exponent may still be difficult to distinguish from 1.5 experimentally. It would thus be interesting to consider other variables in order to discriminate between different theoretical models. Another question is whether this difference obtained with a 2D model survives in three dimensions.

5. Macroscopic scale

The literature on the simulation of plasticity at the macroscopic scale is more scarce, in part because glasses are brittle at the macroscopic scale, their plasticity being mostly limited to the micrometer-scale. However, substantial amounts of plasticity can be reached under conditions of confined plasticity, as in indentation [39, 246]. At the macroscopic scale, simulations are based on the FEM, which requires a constitutive law that relates the plastic strain rate to the state of stress and the history of deformation of the glass.

Following Spaepen [236], most of the early descriptions of the visco-plastic behavior of metallic glasses relied on a flow rule accounting for the evolution of an internal state variable, the free volume. The excess free volume in metallic glasses is usually defined as follows. Let V be the volume of the sample and V_d the volume of the same sample with a dense random packing of atoms. The excess free volume, V_f, is the difference between the two volumes, i.e. $V_\mathrm{f} = V - V_\mathrm{d}$. The flow equation for the plastic shear strain γ derived by Spaepen writes [218, 236]

$$\frac{\partial \gamma}{\partial t} = \nu_0 \exp\left[-\alpha \frac{v^*}{v_\mathrm{f}}\right] \cdot 2 \exp\left[-\frac{\Delta G_0}{k_\mathrm{B} T}\right] \sinh\left[\frac{\sigma \Omega^*}{k_\mathrm{B} T}\right], \tag{22}$$

where ν_0 is an attempt frequency that sets a characteristic time scale. The first exponential is the free-volume contribution (v_f is the average free volume per atom, v^* a critical volume and α a geometrical factor of order unity). The second exponential and the sinh term are derived from a MF stress-biased activation energy model similar to equation (19): ΔG_0 is the shear stress-free activation enthalpy, σ is resolved shear stress and Ω^* the activation volume (the sinh function accounts for both forward and backward shears). This flow rule is complemented by an evolution equation for the free volume assuming a stress-induced production term, a relaxation-induced annihilation term and often a diffusion term. The stress assisted production of free volume has a clear shear thinning effect. The latter effect has been shown early to induce localization [240] (see also the clear presentation of the model and its generalization as well as a linear stability analysis in [110]).

In the very same spirit, Gao [89] recently developed an implicit FEM for simulating inhomogeneous deformation and shear bands of amorphous alloys. The use of a numerical scheme that limits convergence problems in mechanically unstable systems [90] allowed to follow the initiation and propagation of shear bands from local free-volume fluctuations. Two examples are displayed in figure 13. Note that the width of the shear band appears to be controlled only by the lattice discretization length as expected in a model deprived of any internal length scale.

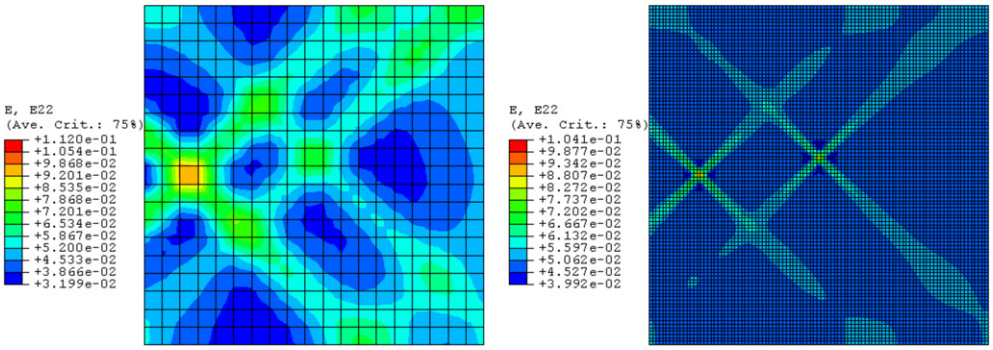

Figure 13. Contour maps of ε_{22} in a uniaxial traction test where the initial free volume has been slightly perturbed at two sites of the lattice. The two lattice sizes shown here illustrate the dependence of the shear band width on the sole mesh size. Reproduced with permission from Gao Y F 2006 *Modelling Simul. Mater. Sci. Eng.* **14** 1329. Copyright (2006) IOP Publishing.

In the recent years, such free-volume based models have been enriched with phenomenological rate- and temperature dependence in the glass transition regime in order to account for the technological thermoplastic forming process [3].

While free volume has been widely used as a shear thinning ingredient, the natural consequence of stress-induced free-volume expansion, i.e. the introduction of an inelastic volumetric deformation, has been less frequently discussed [84, 110]. A simple reason for leaving aside this *a priori* important aspect (after all, while dislocations are volume conserving, no such limit applies to STs) is that in most experimental tests performed on metallic glasses, pressure levels remain low compared with the yield stress value [154]. Strongly contrasting with such a statement is the case of indentation tests where pressure levels are frequently measured in gigapascal units.

So far, two main constitutive laws have been proposed to model plasticity during indentation experiments, one in amorphous silica by Kermouche *et al* [128, 193] and the other in metallic glasses by Anand and Su for low temperatures in the shear banding regime [4, 246] and for high temperatures in the homogeneous deformation regime [5]. The main characteristic of these constitutive laws is to account for the pressure dependence of the plastic deformation of glasses. However, they treat this effect in different ways due to the specificities of the glasses considered. For metallic glasses, the pressure dependence is treated using a Mohr–Coulomb law [142, 154], where the yield stress in shear increases linearly with the normal stress, while for silica glasses, following early attempts based on a simple linearly pressure-dependent Mises criterion [139], a quadratic law involving deviatoric stress and pressure, inspired from the mechanics of porous materials was employed. In both cases, the pressure dependence is related to the free volume in the material but in the case of metallic glasses, plasticity leads to an increase in free volume and a corresponding softening of the glass, whereas in silica glasses, plasticity decreases the free volume and induces densification [118, 282] and hardening [194, 269] of the glass. Finally, in silica glasses, only density hardening was considered (by a linear relation between the plastic limit in hydrostatic compression and the plastic strain) and no hardening in shear was accounted for, while in metallic glasses, shear softening by the increase in free volume was considered, and the Mohr–Coulomb friction coefficient was held constant, implying no density hardening (or softening). The hypothesis used in both constitutive laws are thus quite different but well-adapted to the systems considered since in both cases, the simulations were at least in qualitative agreement with experiments. In particular, in silica glasses, the authors were able to reproduce densification maps below the indentor, while in metallic glasses, the

simulations showed shear band patterns, as shown in figure 1(*c*), in good agreement with experiments and atomic-scale simulations [225, 227]. This comparison is qualitative, but more quantitative comparisons have been made, for instance concerning densification under an indentor [128]. Note also that *in situ* measurements could help for a more detailed comparison between experiments and model predictions [185]. In the perspective of multiscale modeling, the constitutive laws could also be checked directly by MD simulations on submicrometric samples submitted to different kinds of deformations, like shear at constant pressure or hydrostatic compression. Note also that attempts have been made to use rate-and-state models in finite difference simulations of large scale deformations in macroscopic samples [72].

Finally, remaining in the framework of mutiscale modeling, an additional interesting point of comparison is given by recent works simulating the plastic behavior of bulk amorphous matrix composites [142]. In the very same spirit as glass-ceramics developed to improve mechanical properties of oxide glasses, such materials incorporate nano- or micro-particles of a crystalline ductile phase. As strikingly apparent in figure 14, the macroscale plastic deformation of metal-matrix composites strongly recalls mesoscale results discussed above for amorphous materials. In both cases, one recovers similar patterns of criss-crossed shear bands. Such a similarity is obviously not surprising since the very same Eshelby elastic interaction of quadrupolar symmetry is at work in both cases. Beyond the size of the plastic inclusions encountered, note that the main difference between these two otherwise comparable cases stems from the fact that shear bands are persistent in the metal-matrix composites since they are nucleated on well defined structural defects (the ductile particles) while STs experienced at the microscopic scale in glasses are very short-lived.

6. Perspectives and challenges for multiscale modeling

As mentioned in the introduction, the simulations reviewed in this paper at different length scale and time scale were performed mostly independently. Methods and models have now reached a state of development where transfer of information from one scale to the scale above becomes possible. However, there remain challenges that are discussed in the remaining of the section.

6.1. From atomistic to mesoscopic scales

The striking agreement between deformation patterns found in atomistic and mesoscopic simulations, illustrated in figure 10, and the fact that mesoscopic simulations can account for the influence of aging and relaxation of glasses (stress overshoot and shear banding) are clear indications that mesoscopic models are very good tools to check the main ingredients necessary to model plasticity in glasses, such as local visco-plastic events with long-range elasticity. Also, the fact that the same boundary condition effects are found in mesoscopic and atomistic simulations (shear banding favored by fixed boundary conditions) is another proof of the realism of mesoscopic models. Interestingly, both atomistic and mesoscopic models have difficulties reproducing shear banding, which is almost unavoidable at the macroscopic scale, at least at low temperature. The reason is that both atomistic and mesoscopic glass models are far less relaxed than experimental glasses and therefore do not exhibit strong enough structural relaxations and local softening which is the main source of shear bands as seen above.

Mesoscopic models have been used so far mostly phenomenologically. In order to quantitatively transfer information from the atomistic to the mesoscopic scale, several difficult challenges have to be faced. We have identified four main challenges.

- *Length scale.* A mesoscopic model involves a characteristic discretization length scale that must be compared with the other characteristic length scales describing the mechanical

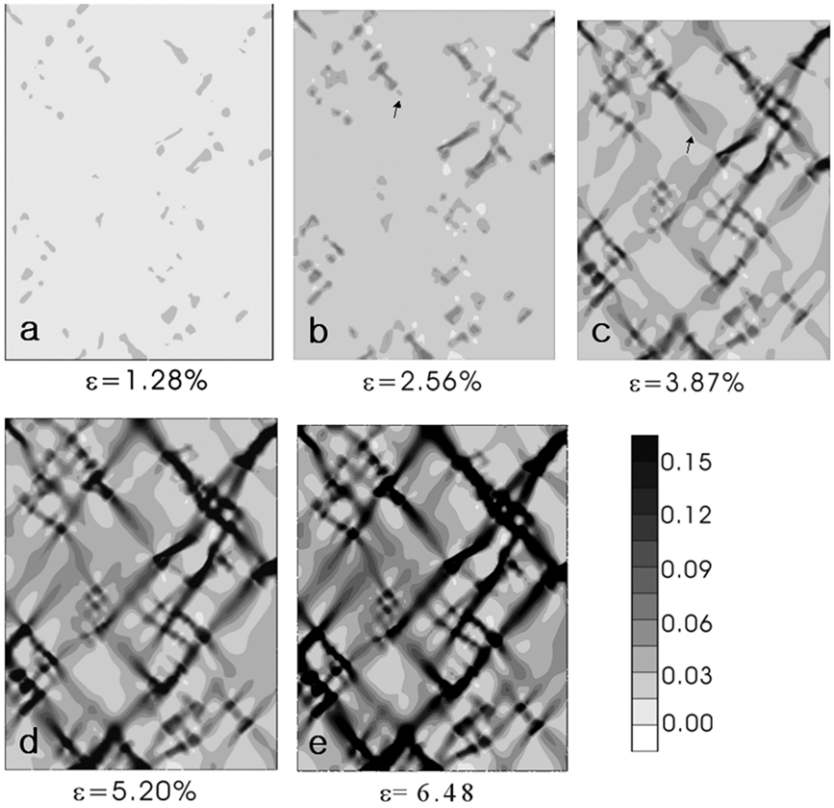

Figure 14. Distribution of the effective strain at various deforming stages of a Ta particle enriched Cu-based bulk amorphous glass matrix; (*a*) 1.3%, (*b*) 2.6%, (*c*) 3.9%, (*d*) 5.2% and (*e*) 6.5%. Reproduced with permission from Lee J C *et al* 2005 *Acta Mater.* **53** 129. Copyright with permission from Elsevier.

response of the system. One of these length scales is the size of the ST itself, ℓ_{ST}. But the choice of the elastic kernel depends on the role devoted to the elastic heterogeneities. In amorphous systems, the typical size for elastic heterogeneities ℓ_{ELAST} is in the nanometer range [75, 150]. This characteristic size has been studied only in specific systems. It has been shown, for example, in 2D LJ systems [262] that linear elasticity is valid only above 5 interatomic distances, and that isotropic and homogeneous elasticity is recovered beyond 20 interatomic distances. The experimental and numerical studies of the vibrational response of different amorphous materials [38, 70, 149, 150, 198, 211, 212, 221, 232] show that disorder affects strongly the acoustical response of materials for wavelengths below a characteristic value λ_{BP} depending on the pressure [166, 178, 181, 239], on the temperature [17, 209], and on the aging time [69], as well as on the precise composition of the material [77]. The order of magnitude of this characteristic wavelength is the nanometer in usual glasses [70, 149, 150, 211] and reflects probably a transition from weak to strong scattering of acoustic waves on strain (or elastic) heterogeneities [210, 257]. It means that homogeneous elasticity cannot be valid at length scales below this characteristic value λ_{BP} [17, 150, 198]. However, visco-plastic rearrangements in mesoscopic models will induce inhomogeneous strains [167] not compatible with the homogeneous elastic kernel usually chosen in the same models. The question of the origin of the nanometer scale for

elastic heterogeneities in amorphous materials and the question of the scale of description for mesoscopic modeling are thus strongly related and of crucial interest to check the validity of the models. Fortunately, it seems that above the scale ℓ_{ELAST}, homogeneous and isotropic elasticity is valid; however, the nanometer scale is precisely the most difficult size to reach experimentally. This is also why an appropriate mesoscopic modeling can be very challenging.

- *Yield criterion.* We have to understand how the ST nucleation criterion, which appears non-local and controlled by elastic moduli (or equivalently, by the stability of the Hessian matrix), may become local and based on stresses at the scale above. Understanding this point is interesting from a fundamental point of view and is also unavoidable in order to develop a physical yield criterion at the micrometer-scale. As seen above, yield stresses in mesoscopic models have so far been either constant or drawn from phenomenological statistical distributions (for instance uniform) without spatial correlations. However, we may expect from the disordered structure of glasses with short- and medium-range orders, that yield stresses should arise from specific distributions that reflect the level of relaxation of the glass and include some spatial correlations. Similarly, energy-based approaches use a homogeneous stress-free activation energy for STs (ΔF_0), with homogeneous ST volume (Ω_0) and strain increment (γ_{p}), while again, we expect these quantities to arise from statistical distributions. This information will have to come from atomistic simulations and will require a better understanding of the relation between the structure and properties of glasses. The first step could be to determine more precisely the nucleation criterion for STs and the relation between the local structure of the glass and its propensity for plastic deformation. One link in metallic glasses could be the fivefold coordinated atoms surrounded by icosahedra that have recently been directly correlated with hard zones under deformation in CuZr glasses [191], but the relation between the local structure and a local yield stress or a local activation energy has yet to be established. Also, such clusters are not relevant to all glasses and a better measure for the local stability of glasses is needed.
- *Time scale.* Mesoscopic models either have no time scale, as the depinning model based on extremal dynamics, or use very simplified dynamics, as the fluidity model based only on two time scales (τ_{pl} and τ_{el}) that are fixed, independent of the local structure of the glass and not clearly related to any microscopic processes. These models can therefore not reproduce the slow dynamics with multiple time scales characteristic of aging glasses, as evidenced by MD simulations near the mode-coupling temperature and by the large energy range of the energy distributions found in glasses at the atomic scale (see figures 2(*d*) and (*e*)). Timescales are also influenced by the temperature, both real and effective. This will require first to better understand the role of temperature and thermal activation at the atomic scale. One way could be through atomistic activated dynamics, based on kinetic Monte Carlo simulations, with distributions of activation energies determined on the fly by saddle-point search methods [204, 281]. Indeed, this technique could simulate aging or plastic deformation on experimental time scales and could be compared with the mesoscopic KMC model.
- *Softening versus hardening.* So far, the treatment of glass microstructure evolution under deformation has been treated very crudely in mesoscopic models, being either simply ignored when a constant yield criterion landscape is used or drawn from phenomenological statistical distributions. On the other hand, we expect that soft regions harden when they deform, for example because their 'free volume' decreases, while strong regions soften because they increase their 'free volume'. Such an effect is qualitatively reproduced when drawing yield stresses from statistical distributions, but we may wish to use more physical distributions. Again, this information will have to come from atomistic simulations and

will require a better understanding of the structure/property relation in glasses. Depending on the microstructure of the glass (pure silica versus soda-lime glass for example), hardening can depend crucially on the geometry of the mechanical deformation (pure shear versus densification or shear at constant pressure) [128]. Also, the origin of polarization and its link to the internal stress field produced by the plastic deformation will have to be better understood to be properly modeled in mesoscopic simulations. The basic question is whether polarization is only related to the stress field accumulated in the structure or is also encrypted in the atomic configurations. In the latter case, an anisotropic softening effect will be required (for instance a yield stress that depends on the sign of the local stress).

6.2. From mesoscopic to macroscopic scales

There is less connection between mesoscopic models and macroscopic constitutive laws. In particular, the two constitutive laws mentioned above are mostly based on the pressure dependence of the mechanical response of glasses, an effect neglected in all mesoscopic models so far. Also, the constitutive laws are based on the notion of free volume and a relation between free volume, yield stress and pressure dependence is assumed. But, if the pressure dependence of the mechanical properties of glasses has been demonstrated at the atomic scale [155, 183, 219], the notion of free volume remains unclear, in particular in metallic glasses where only very little volume change is observed under and after deformation. A first step could therefore be to identify an internal variable that could be characterized at the atomic scale and linked to the mechanical properties, for example related to the distribution of yield stresses. That internal variable will certainly have to be tensorial and not just scalar in order to account for the dependence on pressure and polarization. This information could then be imported in a mesoscopic model that would serve to develop a realistic constitutive law at the macroscopic scale. Different attempts in this direction have already been made in the context of the STZ and SGR theories [79] within the intrinsic assumptions of these theories.

7. Summary and conclusion

Glasses are characterized at the atomistic scale by broad energy spectra and heterogeneities that are consequences of the hierarchical multifunnel structure of their PEL. The latter explains most of the dynamical properties of supercooled liquids and glasses: (i) the strong influence of the quench rate on final glass state, (ii) dynamical heterogeneities, (iii) slow aging process in glassy state and (iv) anelastic recovery after deformation. Plastic deformation in glasses also involves heterogeneities, in the form of local rearrangements that interact elastically, as evidenced by both atomistic and mesoscopic simulations, and we have seen an analogy between string-like events in supercooled liquids and shear transformations in deformed glasses that are both localized rearrangements that allow to system to transit between metabasins.

Glasses relaxed more slowly have more time to explore deeper regions of their PEL. They are more stable thermodynamically (lower potential energy) and kinetically (higher activation energies). They have also a higher mechanical strength with a longer elastic regime and larger elastic moduli. These effects arise naturally in atomistic simulations and are reproduced phenomenologically in mesoscopic models, for instance by increasing the initial level of yield stresses. However, a more quantitative description of this effect at the micrometer scale is still lacking, because it requires a deeper understanding of the dynamics of relaxation and aging in glasses. This is related to a better understanding of the dissipative processes at small scale that are far to be understood in general, as soon as they involve electron–phonon couplings.

Moreover, the effect of bond directionality, already known in crystalline plasticity, is far from being quantitatively understood, as well as the corresponding relation between local structure and plastic damage in amorphous materials, and eventually its mesoscopic description.

Instabilities in the plastic regime are observed at all scales and depend on the way the simulations are carried out. The simplest models, both at the atomistic and mesoscopic scales, do not lead to persistent shear bands. Indeed, in atomistic simulations, unless slow quench rates on MD time scales are used to prepare glasses, or strong interatomic bond directionality, the glass will only undergo transient localizations in the form of elementary shear bands. Similarly, at the mesoscale, we have seen that correlations and disorder can have different origins (dynamical and structural) and that a model without softening, i.e. without structural correlations, but with structural disorder (initial distribution of internal stresses or with stochastic yield stresses) show transient localization patterns, but no permanent shear bands. The other condition to form shear bands is when the glass contains no structural disorder, which explains the strain rate effect of shear banding: shear bands form only when the strain rate is slow enough that the rate of production of structural disorder (which increase with the strain rate) is slower than the relaxation rate of structural disorder. Shear bands are observed in relaxed glasses that exhibit softening, which requires to apply a slow quench at atomistic scale or to include softening effects at the mesoscopic scale. Another way to generate permanent shear bands is to run simulations on covalent systems with strong three-body interactions (bond directionality) at low pressure, because a constant pressure contributes to homogenize the deformation. A better understanding of softening and relaxations at the atomistic and mesoscales is a major issue, which requires to better understand the physics of STs (their nucleation criterion and relation to local softening or hardening). At the macroscopic scale, softening can be included in constitutive laws but the question is what is the relevant internal variable and its corresponding dynamics to represent faithfully the dynamics of STs and of their interactions and relation to softening. At the macroscopic scale, reproducing history-dependence may require to generalize the notions of effective temperature and free volume to transform them into tensorial quantities to reproduce anisotropy and the fact that the symmetry of the plastic strain tensor gets embedded in glass microstructure, leading to anelasticity. Less-relaxed glasses that present a larger density of nucleation sites for plasticity (although the nature of these sites remains elusive, as discussed above) have a lower strength but a higher ductility. This observation is at the basis of several strategies to produce ductile metallic glasses, such as prestraining [143, 286] or ion irradiation [199].

Finally, the question of the temperature dependence of the mechanical response is still largely an open question. Different regimes have been explored, especially the athermal regime and the mean-field regime at higher temperatures. But a relevant description of thermal processes and their competition with mechanical instabilities needs a deeper understanding of the evolution of activation barriers and memory effects in mechanically driven systems and the question of the competition between the dynamics of the numerically chosen thermostat and the local dynamics of the mechanical instabilities makes this question difficult to solve at the moment.

We end with a few open questions that we deem important to answer in order to make significant progress. At the atomic scale, can we identify a geometrical characteristic of weak zones in metallic glasses, more general than coordination defects or special structural environments like icosahedra? Related to temperature, is it possible to quantify properly the respective nucleation and diffusion from a nucleated center of plastic rearrangements? How does the size of the plastic rearrangements depend on the shear rate? What is responsible for the nucleation of large scale rearrangements like elementary shear bands, and do these large scale rearrangements resist thermal activation? Do these large scale events imply non-uniform

temperatures, and local melting that would favor crack propagation? What are the characteristic time scales for structural and mechanical relaxations that must be included in mesoscopic models? All these questions need a more realistic description of the local dissipative processes, that are strongly system-dependent. At the mesoscale, is it possible to find a characteristic length scale for self-consistent mesoscopic models? Which internal variable will account for the specific microscopic structure of the system (for instance, bond directionality), and corresponding relaxations? At the macroscale, is it possible to derive a general constitutive law from microscopic modeling that can take into account the competition between shear and densification, with a complete description of the mechanical history? How does it depend on the specific composition of a glass? The above questions are but a few among a vast list of topics for future research that will benefit from the continuous progress in simulation techniques and experiments, and will hopefully lead to a general understanding and description of glassy mechanics consistent across length- and time-scales.

Acknowledgments

The authors would like to thank Professor Jean-Louis Barrat and Dr Stéphane Roux for helpful discussions and careful reading of the manuscript.

References

[1] Albano F and Falk M L 2005 Shear softening and structure in a simulated three-dimensional binary glass *J. Chem. Phys.* **122** 154508
[2] Allen M P and Tildesley D 1987 *Computer Simulation of Liquids* (Oxford: Clarendon)
[3] Anand L and Hennann D 2008 A constitutive theory for the mechanical response of amorphous metals at high temperatures spanning the glass transition temperature: application to microscale thermoplastic forming *Acta Mater.* **56** 3290–305
[4] Anand L and Su C 2005 A theory for amorphous viscoplastic materials undergoing finite deformations, with application to metallic glasses *J. Mech. Phys. Solids* **53** 1362–96
[5] Anand L and Su C 2007 A constitutive theory for metallic glasses at high homologous temperatures *Acta Mater.* **55** 3735–47
[6] Angelani L, Di Leonardo R, Ruocco G, Scala A and Sciortino F 2000 Saddles in the energy landscape probed by supercooled liquids *Phys. Rev. Lett.* **85** 5356–9
[7] Angelani L, Parisi G, Ruocco G and Viliani G 2000 Potential energy landscape and long-time dynamics in a simple model glass *Phys. Rev.* E **61** 1681–91
[8] Appignanesi G A, Rodriguez Fris J A, Montani R A and Kob W 2006 Democratic particle motion for metabasin transitions in simple glass formers *Phys. Rev. Lett.* **96** 057801
[9] Argon A S 1968 Delayed elasticity in inorganic glasses *J. Appl. Phys.* **39** 4080–6
[10] Argon A S 1979 Plastic deformation in metallic glasses *Acta Metall.* **27** 47–58
[11] Argon A S and Kuo H Y 1979 Plastic flow in a disordered bubble raft *Mater. Sci. Eng.* **39** 101–9
[12] Argon A S and Kuo H Y 1980 Free energy spectra for inelastic deformation of five metallic glass alloys *J. Non-Cryst. Solids* **37** 241–66
[13] Ashby M F and Greer A L 2006 Metallic glasses as structural materials *Scr. Mater.* **54** 321–6
[14] Bacon D, Osetsky Y and Rodney D 2009 Dislocation-obstacle interactions at the atomic level *Dislocations in Solids* vol 15 ed J Hirth and L Kubin (Amsterdam: Elsevier) pp 1–90 chapter 88
[15] Bailey N P, Schiotz J and Jacobsen K W 2004 Simulation of Cu–Mg metallic glass: thermodynamics and structure *Phys. Rev.* B **69** 144205
[16] Bailey N P, Schiotz J, Lemaître A and Jacobsen K W 2007 Avalanche size scaling in sheared three-dimensional amorphous solid *Phys. Rev. Lett.* **98** 095501
[17] Baldi G, Fontana A, Monaco G, Orsingher L, Rols S, Rossi F and Ruta B 2009 Connection between the boson peak and elastic properties in silicate glasses *Phys. Rev. Lett.* **102** 195502
[18] Baret J-C, Vandembroucq D and Roux S 2002 An extremal model of amorphous plasticity *Phys. Rev. Lett.* **89** 195506

[19] Barrat J L and Lemaître A 2010 Heterogeneities in amorphous systems under shear ed L Berthier *et al Dynamical Heterogeneities in Glasses, Colloids, and Granular Media* (Oxford: Oxford University Press)
[20] Bazant M Z and Kaxiras E 1996 Modeling of covalent bonding in solids by inversion of cohesive energy curves *Phys. Rev. Lett.* **77** 4370–3
[21] Bazant M Z, Kaxiras E and Justo J F 1997 Environment-dependent interatomic potential for bulk silicon *Phys. Rev.* B **56** 8542–52
[22] Berthier L and Barrat J L 2002 Nonequilibrium dynamics and fluctuation–dissipation relation in a sheared fluid *J. Chem. Phys.* **116** 6228–42
[23] Berthier L and Barrat J L 2002 Shearing a glassy material: numerical test of nonequilibrium mode-coupling approaches and experimental proposals *Phys. Rev. Lett.* **89** 095702
[24] Berthier L and Biroli G 2011 Theoretical perspective on the glass transition and amorphous materials *Rev. Mod. Phys.* **83** 587
[25] Binder K and Kob W 2005 *Glassy Materials and Disordered Solids: an Introduction to their Statistical Mechanics* (Singapore: World Scientific)
[26] Bocquet L and Ajdari A 2009 Kinetic theory of plastic flow in soft glassy materials *Phys. Rev. Lett.* **103** 036001
[27] Bonamy D 2009 Intermittency and roughening in the failure of brittle heterogeneous materials *J. Phys. D: Appl. Phys.* **42** 214014
[28] Bonn D, Tanase S, Abou B, Tanaka H and Meunier J 2002 Laponite: aging and shear rejuvenation of a colloidal glass *Phys. Rev. Lett.* **89** 015701
[29] Bouchbinder E and Langer J S 2009 Nonequilibrium thermodynamics of driven amorphous materials *Phys. Rev.* E **80** 031131
[30] Broderix K, Bhattacharya K K, Cavagna A, Zippelius A and Giardina I 2000 Energy landscape of a Lennard-Jones liquid: statistics of stationary points *Phys. Rev. Lett.* **85** 5360–4
[31] Büchner S and Heuer A 2000 Metastable states as a key to the dynamics of the supercooled liquids *Phys. Rev. Lett.* **84** 2168–71
[32] Bulatov V V and Argon A S 1994 A stochastic model for continuum elasto-plastic behavior: I. Numerical approach and strain localization *Modelling Simul. Mater. Sci. Eng.* **2** 167
[33] Bulatov V V and Argon A S 1994 A stochastic model for continuum elasto-plastic behavior: II. a study of the glass transition and structural relaxation *Modelling Simul. Mater. Sci. Eng.* **2** 185
[34] Bulatov V V and Argon A S 1994 A stochastic model for continuum elasto-plastic behavior: III. Plasticity in ordered versus disordered solids *Modelling Simul. Mater. Sci. Eng.* **2** 203
[35] Bulatov V V, Abraham F, Kubin L, Devincre B and Yip S 1998 Dislocation junction and crystal plasticity: linking atomistic and mesoscale simulations *Nature* **391** 669
[36] Cancès E, Legoll F, Marinica M C, Minoukadeh K and Willaime F 2009 Some improvements of the activation–relaxation technique method for finding transition pathways on potential energy surfaces *J. Chem. Phys.* **130** 114711
[37] Carré A, Horbach J, Ispas S and Kob W 2008 New fitting scheme to obtain effective potential from Car-Parrinello molecular dynamics simulations: application to silica *Eur. Phys. Lett.* **82** 17001
[38] Champagnon B, Wondraczek L and Deschamps T 2009 Boson peak, structural inhomogeneity, light scattering and transparency of silicate glasses *J. Non-Cryst. Solids* **355** 712
[39] Charleux L, Gravier S, Verdier M, Fivel M and Blandin J J 2006 Indentation plasticity of amorphous and partially crystallized metallic glasses *J. Mater. Res.* **22** 525–32
[40] Chattoraj J, Caroli C and Lemaître A 2010 Universal, additive effect of temperature on the rheology of amorphous solids *Phys. Rev. Lett.* **105** 266001
[41] Chen G L, Liu X J, Hui X D, Hou H K, Yao K F, Liu C T and Wadsworth J 2006 Molecular dynamic simulations and atomic structures of amorphous materials *Appl. Phys. Lett.* **88** 203115
[42] Cheng Y Q, Cao A J and Ma E 2009 Correlation between the elastic modulus and the intrinsic plastic behavior of metallic glasses: the roles of atomic configuration and alloy composition *Acta Mater.* **57** 3253–67
[43] Cheng Y Q, Cao A J, Sheng H W and Ma E 2008 Local order influences initiation of plastic flow in metallic glass: effect of alloy composition and sample cooling history *Acta Mater.* **56** 5263–75
[44] Cloitre M, Borrega R and Leibler L 2000 Rheological aging and rejuvenation in microgel pastes *Phys. Rev. Lett.* **85** 4819–22
[45] Cloitre M, Borrega R, Monti F and Leibler L 2003 Glassy dynamics and flow properties of soft colloidal pastes *Phys. Rev. Lett.* **90** 068303
[46] Coslovich D and Pastore G 2007 Understanding fragility in supercooled Lennard-Jones mixtures: I. locally preferred structures *J. Chem. Phys.* **127** 124504
[47] Coussot P and Grossiord J L (ed) 2002 *Understanding Rheology—From Blood Circulation to Concrete Hardening* (Paris: EDP Sciences)

[48] Coussot P and Ovarlez G 2010 Physical origin of shear-banding in jammed systems *Eur. Phys. J.* E **33** 183–8
[49] Coussot P, Raynaud J S, Bertrand F, Moucheront P, Guilbaud J P, Huynh H T, Jarny S and Lesueur D 2002 Coexistence of liquid and solid phases in flowing soft-glassy materials *Phys. Rev. Lett.* **88** 218301
[50] Cugliandolo L F, Kurchan J and Peliti L 1997 Energy flow, partial equilibration, and effective temperatures in systems with slow dynamics *Phys. Rev.* E **55** 3898–914
[51] Dahmen K, Ertaş D and Ben-Zion Y 1998 Gutemberg-richter and characteristic earthquake behavior in simple-mean-field models of heterogeneous faults *Phys. Rev.* E **58** 1494–501
[52] Dahmen K A, Ben-Zion Y and Uhl J T 2009 Micromechanical model for deformation in solids with universal predictions for stress–strain curves and slip avalanches *Phys. Rev. Lett.* **102** 175501
[53] de Graff A M R and Thorpe M F 2010 The long-wavelength limit of the structure factor of amorphous silicon and vitreous silica *Acta Cryst.* A **66** 22
[54] Debenedetti P G and Stillinger F H 2001 Supercooled liquids and the glass transition *Nature* **410** 259–67
[55] Delogu F 2008 Indentification and characterization of potential shear transformation zones in metallic glasses *Phys. Rev. Lett.* **100** 255901
[56] Demkowicz M J and Argon A S 2004 High-density liquidlike component facilitates plastic flow in a model amorphous silicon system *Phys. Rev. Lett.* **93** 025505
[57] Demkowicz M J and Argon A S 2005 Autocatalytic avalanches of unit inelastic shearing events are the mechanism of plastic deformation in amorphous silicon *Phys. Rev.* B **72** 245206
[58] Denny R A, Reichman D R and Bouchaud J P 2003 Trap model and slow dynamics in supercooled liquids *Phys. Rev. Lett.* **90** 025503
[59] Devincre B, Hoc T and Kubin L 2001 Mesoscopic simulations of plastic deformation *Mater. Sci. Eng.* A **309–310** 211–9
[60] Devincre B, Hoc T and Kubin L 2008 Dislocation mean free paths and strain hardening of crystals *Science* **320** 1745–8
[61] Dimiduk D M, Woodward C, LeSar R and Uchic M D 2006 Scale-free intermittent flow in crystal plasticity *Science* **26** 1188–90
[62] Doliwa B and Heuer A 2003 Energy barriers and activated dynamics in a supercooled Lennard-Jones liquid *Phys. Rev.* E **67** 031506
[63] Doliwa B and Heuer A 2003 Hopping in a supercooled Lennard-Jones liquid: metabasins, waiting time distribution, and diffusion *Phys. Rev.* E **67** 030501
[64] Doliwa B and Heuer A 2003 What does the potential energy landscape tell us about the dynamics of supercooled liquids and glasses? *Phys. Rev. Lett.* **91** 235501
[65] Donati C, Douglas J F, Kob W, Plimpton S J, Poole P H and Glotzer S C 1998 Stringlike cooperative motion in a supercooled liquid *Phys. Rev. Lett.* **80** 2338–42
[66] Donati C D, Glotzer S C, Poole P H, Kob W and Plimpton S J 1999 Spatial correlations of mobility and immobility in a glass-forming Lennard-Jones liquid *Phys. Rev.* E **60** 3107
[67] Doye J P K and Wales D J 2002 Saddle points and dynamics of Lennard-Jones clusters, solids and supercooled liquids *J. Chem. Phys.* **116** 3777–88
[68] Duan G, Xu D, Zhang Q, Zhang G, Cagin T, Johnson W L and Goddard W A III 2005 Molecular dynamics study of the binary $Cu_{46}Zr_{54}$ metallic glass motivated by experiments: glass formation and atomic-level structure *Phys. Rev.* B **71** 224208
[69] Duval A, Etienne S, Simeoni G and Mermet A 2006 Physical aging effect on the boson peak and heterogeneous nanostructure of a silicate glass *J. Non-Cryst. Solids* **352** 4525
[70] Duval A, Mermet A and Saviot L 2007 Boson peak and hybridization of acoustic modes with vibrations of nanometric heterogeneities in glasses *Phys. Rev.* B **75** 024201
[71] Dyre J C 1987 Master-equation approach to the glass transition *Phys. Rev. Lett.* **58** 792–5
[72] Easgate L O, Langer J S and Pechenik L 2003 Dynamics of large-scale plastic deformation and the necking instability in amorphous solids *Phys. Rev. Lett.* **90** 045506
[73] Ediger M D, Angell C A and Nagel S R 1996 Supercooled liquids and glasses *J. Chem. Phys.* **100** 13200–12
[74] Egami T, Dmowski W, Kosmetatos P, Boord M, Tomida T, Oikawa E and Inoue A 1995 Deformation induced bond orientational order in metallic glasses *J. Non-Cryst. Solids* **192 and 193** 591–4
[75] Ehmler H, Heesemann A, Rätzke K and Faupel F 1998 Mass dependence of diffusion in a supercooled metallic melt *Phys. Rev. Lett.* **80** 4919–22
[76] Eshelby J D 1957 The determination of the elastic field of an ellipsoidal inclusion, and related problems *Proc. R. Soc.* A **241** 376
[77] Fabiani E, Fontana A and Buchenau U 2008 Neutron scattering study of the vibrations in silica and germania *J. Chem. Phys.* **128** 244507

[78] Falk M L and Langer J S 1998 Dynamics of viscoplastic deformation in amorphous solids *Phys. Rev.* E **57** 7192–205
[79] Falk M L and Langer J S 2011 Deformation and failure of amorphous solidlike materials *Ann. Rev. Condens. Mater. Phys.* **2** 353–73
[80] Falk M L, Langer J S and Pechenik L 2004 Thermal effects in the shear-transformation-zone theory of amorphous plasticity *Phys. Rev.* E **70** 011507
[81] Falk M L and Maloney C E 2010 Simulating the mechanical response of amorphous solids using atomistic methods *Eur. Phys. J.* B **75** 405–13
[82] Fielding S M, Cates M E and Sollich P 2009 Shear banding, aging and noise dynamics in soft glassy materials *Soft Matter* **5** 2378–82
[83] Fisher D S, Dahmen K and Ben-Zion Y 1997 Statistics of earthquakes in simple models of heterogeneous faults *Phys. Rev. Lett.* **78** 4885–8
[84] Flores K M and Dauskardt R H 2001 Mean stress effects on flow localization and failure in a bulk metallic glass *Acta Mater.* **49** 2527–37
[85] Frenkel D and Smith B 2002 *Understanding Molecular Simulation: from Algorithms to Applications* (San Diego: Academic)
[86] Fusco C, Albaret T and Tanguy A 2010 Role of local order in the small-scale plasticity of model amorphous materials *Phys. Rev.* E **82** 066116
[87] Ganesh P and Widom M 2006 Signature of nearly icosahedral structures in liquid and supercooled liquid copper *Phys. Rev.* B **74** 134205
[88] Ganesh P and Widom M 2008 *Ab initio* simulations of geometrical frustration in supercooled liquid Fe and Fe-based metallic glass *Phys. Rev.* B **77** 014205
[89] Gao Y F 2006 An implicit finite element method for simulating inhomogeneous deformation and shear bands of amorphous alloys based on the free-volume model *Modelling Simul. Mater. Sci. Eng.* **14** 1329–45
[90] Gao Y F and Bower A F 2004 A simple technique for avoiding convergence problems in finite element simulations of crack nucleation and growth on cohesive interfaces *Modelling Simul. Mater. Sci. Eng.* **12** 453–63
[91] Godet J, Pizzagalli L, Brochard S and Beauchamp P 2003 Comparison between classical potentials and *ab initio* methods for silicon under large shear *J. Phys.: Condens. Mater.* **15** 6943–53
[92] Goldstein M 1969 Viscous liquids and the glass transition: a potential energy barrier picture *J. Chem. Phys.* **51** 3728–39
[93] Götze W and Sjögren L 1992 Relaxation processes in supercooled liquids *Rep. Prog. Phys.* **55** 241–376
[94] Gu X J, Poon S J, Shiflet G J and Widom M 2008 Mechanical properties, glass transition temperature, and bond enthalpy trends of high metalloid Fe-based bulk metallic glasses *Appl. Phys. Lett.* **92** 161910
[95] Guckenheimer J and Homes P 1997 *Nonlinear Oscillations, Dynamical Systems, and Bifurcation of Vector Fields* 3rd Edn (New York: Springer)
[96] Han X J and Teichler H 2007 Liquid-to-glass transition in bulk glass-forming $Cu_{60}Ti_{20}Zr_{20}$ alloy by molecular dynamics simulations *Phys. Rev.* E **75** 061501
[97] Harmon J S, Demetriou M D, Johnson W L and Samwer K 2007 Anelastic to plastic transition in metallic glass-forming liquids *Phys. Rev. Lett.* **99** 135502
[98] Hauch J A, Holland D, Marder M P and Swinney H L 1999 Dynamic fracture in single crystal silicon *Phys. Rev. Lett.* **82** 3823–26
[99] Haxton T K and Liu A J 2007 Activated dynamics and effective temperature in a steady state sheared glass *Phys. Rev. Lett.* **99** 195701
[100] Hébraud P and Lequeux F 1998 Mode-coupling theory for the pasty rheology of soft glassy materials. *Phys. Rev. Lett.* **81** 2934–7
[101] Heilmaier M 2001 Deformation behavior of Zr-based metllic glasses *J. Mater. Process Technol.* **117** 374–80
[102] Herschel W H and Bulkley R 1926 Konsistenzmessungen von gummi-benzollosungen *Kolloid Z.* **39** 291
[103] Heuer A 1997 Properties of a glass-forming system as derived from its potential energy landscape *Phys. Rev. Lett.* **78** 4051–5
[104] Heuer A 2008 Exploring the potential energy landscape of glass-forming systems: from inherent structures via metabasins to macroscopic transport *J. Phys.: Condens. Mater.* **20** 373101
[105] Hirth J P and Lothe J 1982 *Theory of Dislocations* (New York: Wiley)
[106] Homer E R, Rodney D and Schuh C A 2010 Kinetic Monte Carlo study of activated states and correlated shear-transformation-zone activity during the deformation of an amorphous metal *Phys. Rev.* B **81** 064204
[107] Homer E R and Schuh C A 2009 Mesoscale modeling of amorphous metals by shear transformation zone dynamics *Acta Mater.* **57** 2823–33

[108] Homer E R and Schuh C A 2010 Three-dimensional shear transformation zone dynamics model for amorphous metals *Model. Simul. Mater. Sci. Eng.* **18** 065009
[109] Huang L and Kieffer J 2003 Molecular dynamics study of cristobalite silica using a charge transfer three-body potential: phase transformation and structural disorder *J. Chem. Phys.* **118** 1487–98
[110] Huang R, Suo Z, Prevost J H and Nix J H 2002 Inhomogeneous deformation in metallic glasses *J. Mech. Phys. Solids* **50** 1011–27
[111] Ilg P and Barrat J L 2007 Driven activation versus thermal activation *Eur. Phys. Lett.* **79** 26001
[112] Inoue A 2000 Stabilization of metallic supercooled liquid and bulk amorphous alloys *Acta Mater.* **48** 279–306
[113] Isner B A and Lacks D J 2006 Generic rugged landscape under strain and the possibility of rejuvenation in glasses *Phys. Rev. Lett.* **96** 025506
[114] Ispas S, Benoit M, Jund P and Jullien R 2002 Structural properties of glassy and liquid tetrasilicate, comparison *ab initio* versus classical force field *J. Non-Cryst. Solids* **351** 1144–50
[115] Ispas S, Zotov N, de Wispaleare S and Kob W 2005 Vibrational properties of a sodium tetrasilicate glass: *ab initio* versus classical force field *J. Non-Cryst. Solids* **351** 1144–50
[116] Jagla E A 2007 Strain localization driven by structural relaxation in sheared amorphous solids *Phys. Rev.* E **76** 046119
[117] Jakse N and Pasturel A 2003 Local order of liquid and supercooled zirconium by *ab initio* molecular dynamics *Phys. Rev. Lett.* **91** 195501
[118] Hui Ji, Keryvin V, Rouxel T and Hammouda T 2006 Densification of window glass under very high pressure and its relevance to vickers indentation *Scr. Mater.* **55** 1159–62
[119] Johari G P and Goldstein M 1970 Viscous liquids and the glass transition. II. secondary relaxations in glasses of rigid molecules *J. Chem. Phys.* **53** 2372–89
[120] Johnson W L 1999 Bulk glass-forming metallic alloys: science and technology *Mater. Res. Soc. Bull.* **24** 42–56
[121] Johnson W L and Samwer K 2005 A universal criterion for plastic yielding of metallic glasses with a $(T/T_g)^{3/2}$ temperature dependence *Phys. Rev. Lett.* **95** 195501
[122] Jónsson H and Andersen H C 1988 Isosahedral ordering in the Lennard-Jones liquid and glass *Phys. Rev. Lett.* **60** 2295–8
[123] Kardar M 1998 Nonequilibrium dynamics of interfaces and lines *Phys. Rep.* **301** 85–112
[124] Karmakar S, Lerner E and Procaccia I 2010 Statistical physics of elasto-plastic steady states in amorphous solids *Phys. Rev.* E **82** 055103
[125] Kawamura Y and Inoue A 2000 Newtonian viscosity of supercooled liquid in a $Pd_{40}Ni_{40}P_{20}$ metallic glass *Appl. Phys. Lett.* **77** 1114–6
[126] Kawasaki T, Araki T and Tanaka H 2007 Correlation between dynamic heterogeneity and medium-range order in two-dimensional glass-forming liquids *Phys. Rev. Lett.* **99** 215701
[127] Kazimirov V Y, Louca D, Widom M, Gu X J, Poon S J and Shiflet G J 2008 Local organization and atomic clustering in multicomponent amorphous steels *Phys. Rev.* B **78** 054112
[128] Kermouche G, Barthel E, Vandembroucq D and Dubujet P 2008 Mechanical modelling of indentation-induced densification in amorphous silica *Acta Mater.* **56** 3222–8
[129] Khonik V, Mitrofanov Y P, Lyakhov S A, Khoviv D A and Kouchakov R A 2009 Recovery of structural relaxation in aged metallic glass as determined by high-precision *in situ* shear modulus measurements *J. Appl. Phys.* **105** 123521
[130] Klement W, Willens R H and Duwez P 1960 Noncrystalline structure in solidified gold–silicon alloys *Nature* **187** 869–70
[131] Kob W and Andersen H C 1995 Testing mode-coupling theory for a supercooled binary Lennard-Jones mixture: the Van Hove correlation function *Phys. Rev.* E **51** 4626–41
[132] Kob W, Donati C, Plimpton S J, Poole P H and Glotzer S C 1997 Dynamical heterogeneities in a supercooled Lennard-Jones liquid *Phys. Rev. Lett.* **79** 2827–31
[133] Kob W, Sciortino F and Tartaglia P 2000 Aging as dynamics in configuration space *Europhys. Lett.* **49** 590
[134] Kobayashi S, Maeda K and Takeuchi S 1980 Computer simulation of atomic structure of $Cu_{57}Zr_{43}$ amorphous alloy *J. Phys. Soc. Japan* **48** 1147–52
[135] Kobayashi S, Maeda K and Takeuchi S 1980 Computer simulation of deformation of amorphous $Cu_{57}Zr_{43}$ *Acta Metall.* **28** 1641–52
[136] Kushima A, Lin X, Li J, Eapen J, Mauro J C, Qian X, Diep P and Yip S 2009 Computing the viscosity of supercooled liquids *J. Chem. Phys.* **130** 224504
[137] Lacks D J 2001 Energy landscape and the non-Newtonian viscoity of liquids and glasses *Phys. Rev. Lett.* **87** 225502
[138] Lacks D J and Osborne M J 2004 Energy landscape picture of overaging and rejuvenation in a sheared glass *Phys. Rev. Lett.* **93** 255501

[139] Lambropoulos J C, Xu S and Fang T 1996 Constitutive law for the densification of fused silica, with applications in polishing and microgrinding *J. Am. Ceram. Soc.* **79** 1441–52
[140] Lançon F, Billard L and Chaudhari P 1986 Thermodynamical properties of a two-dimensional quasicrystal from molecular dynamics calculations *Europhys. Lett.* **2** 625–9
[141] Lauridsen J, Chanan G and Dennin M 2004 Velocity profiles in slowly sheared bubble rafts *Phys. Rev. Lett.* **93** 018303
[142] Lee J C, Kim Y C, Ahn J P and Kim H S 2005 Enhanced plasticity in bulk amorphous matrix composites: macroscopic and microscopic viewpoint studies *Acta Mater.* **53** 129–39
[143] Lee S C, Lee C M, Yang J W and Lee J C 2008 Microstructural evolution of an elastostatically compressed amorphous alloy and its influence on the mechanical properties *Scr. Mater.* **58** 591–4
[144] Lemaître A and Caroli C 2009 Rate-dependent avalanche size in athermally sheared amorphous solids *Phys. Rev. Lett.* **103** 065501
[145] Lemaître A and Caroli C 2006 Dynamical noise and avalanches in quasi-static flow of amorphous materials arXiv:cond-mat/0609689v1
[146] Lemaître A and Caroli C 2007 Plastic response of a two-dimensional amorphous solid to quasistatic shear: transverse particle diffusion and phenomenology of dissipative events *Phys. Rev.* E **76** 036104
[147] Léonforte F 2006 Vibrations et micromécanique de matériaux amorphes modèles *PhD Thesis* Université Lyon 1
[148] Leonforte F, Boissiere R, Tanguy A, Wittmer J P and Barrat J-L 2005 Continuum limit of amorphous elastic bodies III: Three-dimensional systems *Phys. Rev.* B **72** 224206
[149] Leonforte F, Tanguy A and Barrat J-L 2006 Inhomogeneous elastic response of silica glass *Phys. Rev. Lett.* **97** 055501
[150] Leonforte F, Tanguy A, Wittmer J P and Barrat J-L 2002 Continuum limit of amorphous elastic bodies I: A finite-size study of low-frequency harmonic vibrations *Phys. Rev.* B **66** 174205
[151] Leschhorn H, Nattermann T, Stepanow S and Tang L H 1997 Driven interface depinning in a disordered medium *Ann. Phys.* **509** 1–34
[152] Levelut C, Le Parc R, Faivre A, Bruning R, Champagnon B, Martinez V, Simon J P, Bley F and Hazemann J L 2007 Density fluctuations in oxide glasses investigated by small-angle X-ray scattering *J. Appl. Cryst.* **40** S512–S516
[153] Lewandowski J J and Greer A L 2006 Temperature rise at shear bands in metallic glasses *Nature Mater.* **5** 15–8
[154] Lowhaphandu P, Montgomery S L and Lewandowski J J 1999 Effects of superimposed hydrostatic pressure on flow and fracture of a ZrTiNiCuBe bulk amorphous alloy *Scr. Mater.* **41** 19–24
[155] Lund A C and Schuh C A 2003 Yield surface of a simulated metallic glass *Acta Mater.* **51** 5399–411
[156] Madec R, Devincre B, Kubin L, Hoc T and Rodney D 2003 The role of collinear interaction in dislocation-induced hardening *Science* **301** 1879–82
[157] Malandro D L and Lacks D J 1998 Molecular-level mechanical instabilities and enhanced self-diffusion in flowing liquids *Phys. Rev. Lett.* **81** 5576–80
[158] Malandro D L and Lacks D J 1999 Relationships of shear-induced changes in the potential energy landscape to the mechanical properties of ductile glasses *J. Chem. Phys.* **110** 4593–601
[159] Malek R and Mousseau N 2000 Dynamics of Lennard-Jones clusters: a characterization of the activation–relaxation technique *Phys. Rev.* E **62** 7723
[160] Maloney C and Lemaître A 2004 Subextensive scaling in the athermal, quasistatic limit of amorphous matter in plastic shear flow *Phys. Rev. Lett.* **93** 016001
[161] Maloney C and Lemaître A 2004 Universal breakdown of elasticity at the onset of material failure. *Phys. Rev. Lett.* **93** 195501
[162] Maloney C E and Lemaître A 2006 Amorphous systems in athermal, quasistatic shear *Phys. Rev.* E **74** 016118
[163] Maloney C E and Robbins M O 2009 Anisotropic power law strain correlations in sheared amorphous 2D solids *Phys. Rev. Lett.* **102** 225502
[164] Manning M L, Daub E G, Langer J S and Carlson J M 2009 Rate-dependent shear bands in a shear-transformation-zone model of amorphous solids *Phys. Rev.* E **79** 016110
[165] Manning M L, Langer J S and Carlson J M 2007 Strain localization in a shear transformation zone model for amorphous solids *Phys. Rev.* E **76** 056106
[166] Mantisi B *et al* 2010 Non-Debye normalization of the glass vibrational density of states in mildly densified silicate glasses *J. Phys.: Condens. Mater.* **22** 025402
[167] Martens K, Bocquet L and Barrat J L 2011 Connecting diffusion and dynamical heterogeneities in actively deformed amorphous systems *Phys. Rev. Lett.* **106** 156001
[168] Mayr S G 2006 Activation energy of shear transformation zones: a key for understanding rheology of glasses and liquids *Phys. Rev. Lett.* **97** 195501

[169] Mendelev M I, Kramer M J, Ott R T, Sordelet D J, Yagodin D and Popel P 2009 Development of suitable interatomic potentials for simulation of liquid and amorphous Cu–Zr alloys *Phil. Mag.* **89** 967–87
[170] Mendelev M I, Sordelet D J and Kramer M J 2007 Using atomistic computer simulations to analyze x-ray diffraction data from metallic glasses *J. Appl. Phys.* **102** 043501
[171] Micoulaut M, Guissani Y and Guillot B 2006 Simulated structural and thermal properties of glassy and liquid germania *Phys. Rev.* E **73** 031504
[172] Middleman S 1962 *The Flow of High Polymers* (New York: Academic)
[173] Middleton T F and Wales D J 2001 Energy landscape of some model glass formers *Phys. Rev.* B **64** 024205
[174] Miguel M C, Vespignani A, Zapperi S, Weiss J and Grasso J-R 2001 Intermittent dislocation flow in viscoplastic deformation *Nature* **410** 667–71
[175] Miller R E and Rodney D 2008 On the nonlocal nature of dislocation nucleation during nanoindentation *J. Mech. Phys. Solids* **56** 1203–23
[176] Miller R E and Tadmor E B 2009 A unified framework and performance benchmark of fourteen multiscale atomistic/continuum coupling methods *Modelling Simul. Mater. Sci. Eng.* **17** 053001
[177] Mokshin A and Barrat J L 2008 Shear induced crystallization of an amorphous system *Phys. Rev.* E **77** 021505
[178] Monaco A, Chumakov A I, Monaco G, Crichton W A, Meyer A, Comez L, Fioretto D, Korecki J and Rüffer R 2006 Effect of densification on the density of vibrational states of glasses *Phys. Rev. Lett.* **97** 135501
[179] Moorcroft R L, Cates M E and Fielding S M 2011 Age-dependent transient shear banding in soft glasses *Phys. Rev. Lett.* **106** 055502
[180] Muskhelishvili N I 1953 *Some Basic Problems of the Mathematical Theory of Elasticity* (Groningen: Kluwer)
[181] Niss K, Begen B, Frick B, Ollivier J, Beraud A, Sokolov A and Alba-Simionesco S 2007 Influence of pressure on the boson peak: stronger than elastic medium transformation *Phys. Rev. Lett.* **99** 055502
[182] Nogaret T, Rodney D, Fivel M and Robertson C 2008 Clear band formation simulated by dislocation dynamics: role of helical turns and pile-ups *J. Nucl. Mater.* **380** 22–9
[183] Ogata S, Shimizu F, Li J, Wakeda M and Shibutani Y 2006 Atomistic simulation of shear localization in Cu–Zr bulk metallic glass *Intermetallics* **14** 1033–7
[184] Ono I K, O'Hern C S, Durian D J, Langer S A, Liu A J and Nagel S R 2002 Effective temperatures of a driven system near jamming *Phys. Rev. Lett.* **89** 095703
[185] Ott R T, Sansoz F, Molinari J F, Ramesh K T and Hufnagel T 2005 Micro-mechanics of deformation of metallic-glass-matrix composites from *in-situ* strain synchrotron measurements and finite element modeling *Acta Mater.* **53** 1883–93
[186] Ott R T, Heggen M, Feuerbacher M, Park E S, Kim D H, Kramer M J, Besser M F and Sordelet D J 2008 Anelastic strain and structural anisotropy in homogeneously deformed $Cu_{64.5}Zr_{35.5}$ metallic glass *Acta Mater.* **56** 5575–83
[187] Ovarlez G, Rodts S, Chateau X and Coussot P 2009 Phenomenology and physical origin of shear localization and shear banding in complex fluids *Acta Rheol.* **48** 831–44
[188] Paczuski M, Maslov S and Bak P 1996 Avalanche dynamics in evolution, growth, and depinning models *Phys. Rev.* E **53** 414–43
[189] Park K W, Jang J, Wakeda M, Shibutani Y and Lee J C 2007 Atomic packing density and its influence on the properties of Cu–Zr amorphous alloys *Scr. Mater.* **57** 805–8
[190] Pedersen U R, Schrøder T B, Dyre J C and Harrowell P 2010 Geometry of slow structural fluctuations in a supercooled binary alloy *Phys. Rev. Lett.* **104** 105701
[191] Peng H L, Li M Z and Wang W H 2011 Structural signature of plastic deformation in metallic glasses *Phys. Rev. Lett.* **106** 135503
[192] Peng H L, Li M Z, Wang W H, Wang C Z and Ho K M 2010 Effect of local structures and atomic packing on glass forming ability in Cu_xZr_{100-x} metallic glasses *Appl. Phys. Lett.* **96** 021901
[193] Perriot A, Barthel E, Kermouche G, Quérel G and Vandembroucq D 2011 On the plastic deformation of soda-lime glass—a Cr^{3+} luminescence study of densification *Phil. Mag.* **91** 1245–55
[194] Perriot A, Martinez V, Martinet C, Champagnon B, Vandembroucq D and Barthel E 2006 Raman micro-spectroscopic map of plastic strain in indented amorphous silica *J. Am. Ceram. Soc.* **89** 596–601
[195] Phillips R, Rodney D, Shenoy V, Tadmor E and Ortiz M 1999 Hierarchical models of plasticity: dislocation nucleation and interaction *Modelling Simul. Mater. Sci. Eng.* **7** 769
[196] Picard G, Ajdari A, Lequeux F and Bocquet L 2004 Elastic consequences of a single plastic event: A step towards the microscopic modeling of the flow of yield stress fluids *Eur. Phys. J.* E **15** 371–81
[197] Picard G, Ajdari A, Lequeux F and Bocquet L 2005 Slow flows of yield stress fluids: complex spatio-temporal behaviour within a simple elasto-plastic model *Phys. Rev.* E **71** 010501(R)

[198] Pilla O, Fontana A, Gonçalvez J R, Montagna M, Rossi F, Viliani G, Angelani L, Ruocco G, Monaco G and Sette F 2004 The low energy excess of vibrational sates in a-SiO_2: the role of transverse dynamics *J. Phys.: Condens. Mater.* **16** 8519

[199] Raghavan R, Boopathy K, Ghisleni R, Pouchon M A, Ramamurty U and Michler J 2010 Ion irradiation enhances the mechanical performance of metallic glasses *Scr. Mater.* **62** 462–5

[200] Reger-Leonhard A, Heilmaier M and Eckert J 2000 Newtonian flow of $Zr_{55}Cu_{30}Al_{10}Ni_5$ bulk metallic glassy alloys *Scr. Mater.* **43** 459–64

[201] Richeton T, Dobron P, Chmelik F, Weiss J and Louchet F 2006 On the critical character of plasticity in metallic single crystals *Mater. Sci. Eng.* A **424** 190–5

[202] Richeton T, Weiss J and Louchet F 2006 Dislocation avalanches: role of temperature, grain size and strain hardening *Acta Mater.* **53** 4463–71

[203] Rodney D and Schuh C 2009 Distribution of thermally activated plastic events in a flowing glass *Phys. Rev. Lett.* **102** 235503

[204] Rodney D and Schuh C A 2009 Yield stress in metallic glasses: the jamming-unjamming transition studied through Monte Carlo simulations based on the activation–relaxation technique *Phys. Rev.* B **80** 184203

[205] Rottler J and Robbins M O 2001 Yield conditions for deformation of amorphous polymer glasses *Phys. Rev.* E **64** 051801

[206] Rottler J and Robbins M O 2003 Shear yielding of amorphous glassy solids: Effect of temperature and strain rate *Phys. Rev.* E **68** 011507

[207] Rottler J and Robbins M O 2005 Unified description of aging and rate effects in yield of glassy solids *Phys. Rev. Lett.* **95** 225504

[208] Rountree C L, Vandembroucq D, Talamali M, Bouchaud E and Roux S 2009 Plasticity-induced structural anisotropy of silica glass *Phys. Rev. Lett.* **102** 195501

[209] Rufflé B, Ayrinhac S, Courtens E, Vacher R and Foret M 2010 Scaling the T-dependent boson peak of vitreous silica with the high-frequency bulk modulus derived from Brillouin scattering data *Phys. Rev. Lett.* **104** 067402

[210] Rufflé B, Foret M, Courtens E, Vacher R and Monaco G 2003 Observation of the onset of strong scattering on high frequency acoustic phonons in densified silica glass *Phys. Rev. Lett.* **90** 095502

[211] Rufflé B, Guimbretiere G, Courtens E and Vacher R 2006 Glass specific behavior in the damping of acoustic-like vibrations *Phys. Rev. Lett.* **96** 045502

[212] Rufflé B, Parshin D A, Courtens E and Vacher R 2008 Boson peak and its relation to acoustic attenuation in glasses *Phys. Rev. Lett.* **100** 015501

[213] Russo J and Sciortino F 2010 How do self-assembling polymers and gels age compared to glasses? *Phys. Rev. Lett.* **104** 195701

[214] Sastry S, Debenedetti P G and Stillinger F H 1998 Signatures of distinct dynamical regimes in the energy landscape of a glass-forming liquid *Nature* **393** 554–7

[215] Sastry S, Debenedetti P G, Stillinger F H, Schroder T B, Dyre J C and Glotzer S C 1999 Potential energy landscape signature of slow dynamics in glass forming liquids *Physica* A **270** 301–8

[216] Schroder T B, Sastry S, Dyre J C and Glotzer S C 2000 Crossover to potential energy landscape dominated dynamics in a model glass-forming liquid *J. Chem. Phys.* **112** 9834–40

[217] Schroers J and Johnson W L 2004 Ductile bulk metallic glass *Phys. Rev. Lett.* **93** 255506

[218] Schuh C A, Hufnagel T C and Ramamurty U 2007 Mechanical behavior of amorphous alloys *Acta Mater.* **55** 4067–109

[219] Schuh C A and Lund A C 2003 Atomistic basis for the plastic yield criterion of metallic glasses *Nature Mater.* **2** 449–52

[220] Sciortino F, Kob W and Tartaglia P 1999 Inherent structure entropy of supercooled liquids *Phys. Rev. Lett.* **83** 3214–8

[221] Sette F, Krisch M, Masciovecchio C, Ruocco G and Monaco G 1998 Dynamics of glasses and glass-forming liquids studied by inelastic x-ray scattering *Science* **280** 1550–5

[222] Sheng H W, Luo W K, Alamgir F M, Bai J M and Ma E 2006 Atomic packing and short-to-medium-range order in metallic glasses *Nature* **439** 419–25

[223] Shenoy V, Miller R, Tadmor E, Rodney D, Phillips R and Ortiz M 1999 An adaptive finite element approach to atomic-scale mechanics: the quasicontinuum method *J. Mech. Phys. Solids* **47** 611–42

[224] Shi Y and Falk M L 2005 Strain localization and percolation of stable structure in amorphous solids *Phys. Rev. Lett.* **95** 095502

[225] Shi Y and Falk M L 2005 Structural transformation and localization during simulated nanoindentation of a noncrystalline metal film *Appl. Phys. Lett.* **86** 011914

[226] Shi Y and Falk M L 2006 Atomic-scale simulations of strain localization in three-dimensional model amorphous solids *Phys. Rev.* B **73** 214201
[227] Shi Y and Falk M L 2007 Stress-induced structural transformation and shear banding during simulated nanoindentation of a metallic glass *Acta Mater.* **55** 4317–24
[228] Shi Y, Katz M B, Li H and Falk M L 2007 Evaluation of the disorder temperature and free-volume formalisms via simulations of shear banding in amorphous solids *Phys. Rev. Lett.* **98** 185505
[229] Shintani H and Tanaka H 2006 Frustration on the way to crystallization in glass *Nature Phys.* **2** 200–6
[230] Shorey A, Xin K, Chen K H and Lambropoulos J C 1998 Deformation of fused silica: nanoindentation and densification *Proc. SPIE* **3424** 72–81
[231] Simmons J H, Ochoa R, Simmons K D and Mills J J 1988 Non-Newtonian viscous flow in soda-lime-silica glass at forming and annealing temperatures *J. Non-Cryst. Solids* **105** 313
[232] Sintani H and Tanaka H 2008 Universal link between the boson peak and transverse phonons in glass *Nature Mater.* **7** 870
[233] Sneppen K 1992 Self-organized pinning and interface growth in a random medium *Phys. Rev. Lett.* **69** 3539–42
[234] Sollich P 1998 Rheological constitutive equation for a model of soft glassy materials *Phys. Rev.* E **58** 738–59
[235] Sollich P, Lequeux F, Hébraud P and Cates M E 1997 Rheology of soft glassy materials *Phys. Rev. Lett.* **78** 2020–3
[236] Spaepen F 1977 Microscopic mechanism for steady-state inhomogeneous flow in metallic glasses *Acta Metall.* **25** 407–15
[237] Srolovitz D, Egami T and Vitek V 1981 Radial distribution function and structural relaxation in amorphous solids *Phys. Rev.* B **24** 6936–44
[238] Srolovitz D, Vitek V and Egami T 1983 An atomistic study of deformation of amorphous metals *Acta Metall.* **31** 335–52
[239] Starviou E, Raptis C and Syassen K 2010 Effects of pressure on the boson peak of tellurite $(TeO_2)_{1-x}(ZnO)_x$ glasses: evidence of an elastic glass to glass transition *Phys. Rev.* B **81** 174202
[240] Steif P S, Spaepen F and Hutchinson J W 1982 Strain localization in amorphous metals *Acta Metall.* **30** 447–55
[241] Stevenson J D, Schmalian J and Wolynes P G 2006 The shapes of cooperatively rearranging regions in glass-forming liquids *Nature Phys.* **2** 268–74
[242] Stillinger F H 1995 A topographic view of supercooled liquids and glass formation *Science* **267** 1935–9
[243] Stillinger F H and Weber T A 1984 Packing structures and transitions in liquids and solids *Science* **225** 983–9
[244] Stillinger F H and Weber T A 1985 Computer simulation of local order in condensed phases of silicon *Phys. Rev.* B **31** 5262
[245] Struik L C E 1978 *Physical Aging in Amorphous Polymers and other Materials* (Amsterdam: Elsevier)
[246] Su C and Anand L 2006 Plane strain indentation of a Zr-based metallic glass: experiments and numerical simulation *Acta Mater.* **54** 179–89
[247] Sun B A, Yu H B, Jiao W, Zhao D Q and Wang W H 2010 Plasticity of ductile metallic glasses: A self organized critical state *Phys. Rev. Lett.* **105** 035501
[248] Suzuki Y, Haimovich J and Egami T 1987 Bond-orientational anisotropy in metallic glasses observed by x-ray diffraction *Phys. Rev.* B **35** 2162–8
[249] Talamali M, Petäjä V, Roux S and Vandembroucq D 2008 Path independent integrals to identify two-dimensional localized plastic events *Phys. Rev.* E **78** 016109
[250] Talamali M, Petäjä V, Vandembroucq D and Roux S 2010 Strain localization and anisotropic correlations in a mesoscopic model of amorphous plasticity arXiv:1005.2463
[251] Talamali M, Petäjä V, Vandembroucq D and Roux S 2011 Avalanches, precursors and finite size fluctuations in a mesoscopic model of amorphous plasticity *Phys. Rev.* E **84** 016115
[252] Talati M, Albaret T and Tanguy A 2009 Atomistic simulations of elastic and plastic properties in amorphous silicon *Europhys. Lett.* **86** 66005
[253] Tanaka H, Kawasaki T, Shintani H and Watanabe K 2010 Critical-like behaviour of glass-forming liquids *Nature Mater.* **9** 324–31
[254] Tang H S and Kalyon D M 2004 Estimation of the parameters of Herschel–Bulkley fluid under wall slip using a combination of capillary and squeeze flow viscometers *Rheol. Acta* **43** 80–8
[255] Tanguy A, Gounelle M and Roux S 1998 From individual to collective pinning: effect of long-range elastic interactions *Phys. Rev.* E **58** 1577–90
[256] Tanguy A, Leonforte F and Barrat J L 2006 Plastic response of a 2D Lennard-Jones amorphous solid: detailed analyses of the local rearrangements at very slow strain rate *Eur. Phys. J.* E **20** 355–64
[257] Tanguy A, Mantisi B and Tsamados M 2010 Vibrational modes as a predictor for plasticity in a model glass *Europhys. Lett.* **90** 16004

[258] Tarjus G, Kivelson S A, Nussinov Z and Viot P 2005 The frustration-based approach of supercooled liquids and the glass transition: a review and critical assessment *J. Phys.: Condens. Mater.* **17** R1143–82
[259] Tersoff J 1988 Empirical interatomic potential for silicon with improved elastic properties *Phys. Rev.* B **38** 9902–5
[260] Tomida T and Egami T 1993 Molecular-dynamics study of structural anisotropy and anelasticity in metallic glasses *Phys. Rev.* B **48** 3048–57
[261] Tsamados M 2010 Plasticity and dynamical heterogeneity in driven glassy materials *Eur. Phys. J.* E **32** 165–81
[262] Tsamados M, Tanguy A, Goldenberg C and Barrat J L 2009 Local elasticity map and plasticity in a model Lennard-Jones glass *Phys. Rev.* E **80** 026112
[263] Tsamados M, Tanguy A, Léonforte F and Barrat J L 2008 On the study of local-stress rearrangements during quasi-static plastic shear of a model glass: do local-stress components contain enough information? *Eur. Phys. J.* E **26** 283–93
[264] Tsuneyuki S, Tsukada M, Aoki H and Matsui Y 1988 First-principles interatomic potential of silica applied to molecular dynamics *Phys. Rev. Lett.* **61** 869–72
[265] Utz M, Debenedetti P and Stillinger F H 2000 Atomistic simulation of aging and rejuvenation in glasses *Phys. Rev. Lett.* **84** 1471–5
[266] Valiquette F and Mousseau N 2003 Energy landscape of relaxed amorphous silicon *Phys. Rev.* B **68** 125209
[267] van Beest B W H, Kramer G J and van Santen R A 1990 Force fields for silicas and aluminophosphates based on *ab initio* calculations *Phys. Rev. Lett.* **64** 1955
[268] Van Kampen N 1992 *Stochastic Processes in Physics and Chemistry* (Amsterdam: North-Holland)
[269] Vandembroucq D, Deschamps T, Coussa C, Perriot A, Barthel E, Champagnon B and Martinet C 2008 Density hardening plasticity and mechanical aging of silica glass under pressure: a Raman spectroscopic study *J. Phys.: Condens. Mater.* **20** 485221
[270] Vandembroucq D and Roux S 2011 Mechanical noise dependent aging and shear banding behavior of a mesoscopic model of amorphous plasticity arXiv:1104.4863
[271] Vandembroucq D and Roux S 2011 Shear banding behavior in glasses: a mesoscopic approach unpublished
[272] Vandembroucq D, Skoe R and Roux S 2004 Universal fluctuations of depinning forces, application to finite temperature behavior *Phys. Rev.* E **70** 051101
[273] Varnik F, Bocquet L, Barrat J L and Berthier L 2003 Shear localization in a model glass *Phys. Rev. Lett.* **90** 095702
[274] Varnik F and Raabe D 2008 Profile blunting and flow blockage in a yield-stress fluid: A molecular dynamics study *Phys. Rev.* E **77** 011504
[275] Viasnoff V and Lequeux F 2002 Rejuvenation and overaging in a colloidal glass under shear *Phys. Rev. Lett.* **89** 065701
[276] Wahnström G 1991 Molecular-dynamics study of a supercooled two-component Lennard-Jones system *Phys. Rev.* A **44** 3752–64
[277] Wales D J 2003 *Energy Landscapes* (Cambridge: Cambridge University Press)
[278] Wales D J, Miller M A and Walsh T R 1998 Archetypal energy landscapes *Nature* **394** 758–60
[279] Widmer-Cooper A and Harrowell P 2006 Predicting the long-time dynamic heterogeneity in a supercooled liquid on the basis of short-time heterogeneities *Phys. Rev. Lett.* **96** 185701
[280] Widmer-Cooper A, Perry H, Harrowell P and Reichman D R 2008 Irreversible reorganization in a supercooled liquid originates from localized soft modes *Nature Phys.* **4** 711–5
[281] Xu L and Henkelman G 2008 Adaptive kinetic Monte Carlo for first-principles accelerated dynamics *J. Chem. Phys.* **129** 114104
[282] Yoshida S, Rouxel T and Sangleboeuf J C 2006 Quantitative evaluation of indentation-induced densification in glass *J. Mater. Res.* **55** 1159–62
[283] Zaiser M 2006 Scale invariance in plastic flow of crystalline solids *Adv. Phys.* **55** 185–245
[284] Zaiser M and Moretti P 2005 Fluctuation phenomena in crystal plasticity—a continuum model *J. Stat. Mech.* **2005** P08004
[285] Zaiser M and Nikitas P 2007 Slip avalanches in crystal plasticity: scaling of the avalanche cut-off *J. Stat. Mech.* **2007** P04013
[286] Zhang Y, Wang W H and Greer A L 2006 Making metallic glasses plastic by control of residual stress *Nature Mater.* **5** 857–60
[287] Zhang Z F, Eckert J and Schultz L 2003 Difference in compressive and tensile fracture mechanisms of $Rr_{59}Cu_{20}Al_{10}Ni_8Ti_3$ bulk metallic glass *Acta Mater.* **51** 1167–79
[288] Zink M, Samwer K, Johnson W L and Mayr S G 2006 Plastic deformation of metallic glasses: size of shear transformation zones from molecular dynamics simulations *Phys. Rev.* B **73** 172203